REHABILITATION OF WOODEN UTILITY POLES WITH SPRAYED-GFRP COMPOSITES

By:

Shukai Chen

A Thesis submitted to the Faculty of Graduate Studies of
The University of Manitoba
in partial fulfillment of the requirement for the degree of

MASTER OF SCIENCE

Department of Civil Engineering
University of Manitoba
Winnipeg, Manitoba

ABSTRACT

Wooden utility poles have been used for over a century due to their sustainability, accessibility, excellent nonconducting properties, and construction flexibility. However, the main problem is the loss of load-carrying capacity, which is caused by decay. Rehabilitation techniques were investigated to extend the service life of wooden poles including steel trusses and wrapping with externally bonded (EB) fibre-reinforced polymer (FRP) laminates. Although the performance of the EB-FRP was reported to be prominent, the installation procedures are complicated, and it has associated debonding issues. To overcome these issues while maintaining the benefits of the FRP material, the sprayed-FRP composites technique is introduced in this study. This research aims at evaluating the performance of sprayed glass FRP (GFRP) composites and near-surface mounted (NSM) GFRP bars in rehabilitation of wooden utility poles. The mechanical properties, bond performance, and confinement effects of the sprayed-GFRP composites were determined. Then an analytical procedure was developed to predict the load carrying capacity of wooden poles retrofitted with sprayed-GFRP. To verify the predicted capacities, twelve 6.7 m-long (22 ft) wood poles were rehabilitated with sprayed-GFRP composites and/or NSM-GFRP bars (No. 10) and tested under monotonic horizontal loading up to failure. The test parameters include the sprayed-GFRP coating thickness (4, 6, and 8 mm), the sprayed-GFRP coating length (1.0 and 2.0 m), and the rehabilitation technique (sprayed-GFRP composites and NSM-GFRP bars).

The results showed that using the sprayed-GFRP layer to restore the load-carry capacity of the old and damaged poles is a feasible rehabilitation method that can strengthen the old poles to reach even a higher load-carry capacity than their original one, given that the length of the

sprayed layer is sufficient. In addition, the load-carrying capacity of the retrofitted poles was not affected by the increase of the sprayed-GFRP thickness beyond 6 mm. Therefore, it was deemed that using 6-mm thick sprayed-GFRP composites to rehabilitate wooden utility poles is a cost-effective rehabilitation option. Moreover, the results also showed that using NSM-GFRP bars solely to rehabilitate damaged poles is not cost-effective or structurally efficient compared to the sprayed-GFRP composites.

ACKNOWLEDGEMENT

I would like to acknowledge the contributions of the following institutions and individuals without whom this project would not be conducted successfully:

- My advisor, Dr. Ehab El-Salakawy, PhD, PEng, FACI, FCSCE, FEIC, FIIFC, Professor of Structural Engineering in the Department of Civil Engineering at the University of Manitoba, for his support and guidance throughout the duration of this research project.
- The technical staff at the W.R. McQuade Structures Laboratory, Dr. Chad Klowak, Mr. Samuel Abraha, and Mr. Daniel Szara, for their technical assistance in the laboratory testing.
- Natural Sciences and Engineering Research Council of Canada (NSERC), for the financial support for this research project.
- Manitoba Hydro, for providing financial support, pole specimens, and wood filler materials for this research project.
- Carlson Commercial & Industrial Services Ltd., for providing the sprayed-GFRP composites and the spraying services.
- Mr. Simons Scott (Manitoba Hydro), for providing information regarding wooden utility poles and wood filler materials.
- Dr. Amr E. Abdallah, PhD, EIT, for his help on results discussion, summary, and review.
- My family for their unconditional support, both financially and psychologically.

TABLE OF CONTENTS

ABSTRACT i
ACKNOWLEDGEMENT iii
TABLE OF CONTENTS iv
LIST OF TABLES vii
LIST OF FIGURES viii
LIST OF NOTATIONS xi
CHAPTER 1 – INTRODUCTION 1
1.1 Background 1
1.2 Research Significance 4
1.3 Research Objectives 4
1.4 Scope of Work 5
1.5 Methodology 6
1.6 Thesis layout 6
CHAPTER 2 – LITERATURE REVIEW 8
2.1 General 8
2.2 Wood Rehabilitation 9
2.2.1 Existing rehabilitation techniques for wooden poles 9
2.2.2 Fibre-reinforced polymer for rehabilitation of wood members 12
2.3 Sprayed-FRP Techniques and Applications 16
2.3.1 Sprayed-FRP systems 16
2.3.2 Sprayed-FRP in structural rehabilitation 17
2.4 Literature Review Summary 20
2.4.1 Sprayed-GFRP coating thickness 21
2.4.2 Sprayed-GFRP coating length 21
2.4.3 Bonding adhesive 22
CHAPTER 3 - PHASE I: MATERIAL TESTS FOR SPRAYED-GFRP COMPOSITES 23
3.1 General 23
3.2 Materials and Application Procedures 23
3.2.1 GFRP composites 23

3.2.2 Bonding adhesives 24
3.3 Coupon Tests 26
3.3.1 Test specimens and methods 26
3.3.2 Test setup and instrumentation 28
3.3.3 Test results and discussion 30
3.4 Pull-off Tests 36
3.4.1 Test specimens and methods 37
3.4.2 Test setup and procedure 40
3.4.3 Test results and discussion 42
3.5 Confinement Tests 46
3.5.1 Test specimens and methods 46
3.5.2 Test setup and procedure 47
3.5.3 Test results and discussion 48
CHAPTER 4 - PHASE II: WOOD POLES TESTS 53
4.1 General 53
4.2 Materials 53
4.3 Specimens Details and Construction Process 55
4.3.1 Test matrix 55
4.3.2 Series I – Control specimens 57
4.3.3 Series II 57
4.3.4 Series III 58
4.3.5 Rehabilitation process 61
4.4 Test Setup and Procedure 62
4.5 Instrumentation 67
4.6 Test Results and Discussion 67
4.6.1 Adjusted code requirements for horizontal load capacity 67
4.6.2 Series I – Control Specimens 69
4.6.3 Load-carrying capacities and failure modes – Series II poles 70
4.6.4 Load-deflection relationship – Series II poles 74
4.6.5 Load-carrying capacities and failure modes – Series III poles 75
4.6.6 Load-deflections relationships – Series III poles 81
4.6.7 NSM-GFRP bars strains 83

CHAPTER 5 – ANALYTICAL MODEL FOR LOAD CAPACITY AND FAILURE MODE PREDICTION 86
5.1 Horizontal Load Capacity Prediction 86
5.1.1 Contribution of Poles 86
5.1.2 Contribution of GFRP Composite 87
5.2 Comparisons against Experimental Data and Model Refinement 90
5.3 Simplified Design Model 91
CHAPTER 6 – CONCLUSIONS AND RECOMMENDATIONS 92
6.1 Conclusions 92
6.2 Recommendations for Future Work 95
REFERENCES 96

LIST OF TABLES

Table 3.1: Ingredients of 100 g n-HMR solution.....25
Table 3.2: Dimension details and test type of all sprayed-GFRP coupons.....26
Table 3.3: Test results of tension coupons.....32
Table 3.4: Test results of compression coupons.....34
Table 3.5: Test results of shear coupons.....36
Table 3.6: Pull-off test matrix and test results.....40
Table 3.7: Confinement test matrix.....47
Table 3.8: Test results of the normal-strength concrete cylinders.....49
Table 3.9: Test results of the high-strength concrete cylinders.....49
Table 4.1: Wood pole details.....54
Table 4.2: Test matrix.....57
Table 4.3: Horizontal Load Requirements.....68
Table 4.4: Test results for Series II poles.....71
Table 4.5: Test results for Series III poles.....75
Table 5.1: Predicted and proposed load capacities for Series II poles.....88
Table 5.2: Predicted load capacities for Series III poles.....89

LIST OF FIGURES

Figure 2.1: Osmose products, (a) Osmo-C-Truss, (b) Osmo-C2-Truss, and (c) FiberWrap™ II (Osmose 2022).....9
Figure 2.2: Laminated Wood Systems products, (a) PhaseRaiser® system, (b) PRS – Pole Reclassification System®, and (c) PoleEnforcer® Spliced Reinforcement System (SRS).....12
Figure 3.1: Components of the GFRP spray machine, (a) Spray machine, and (b) Spray gun.....24
Figure 3.2: Shear test coupon specimens: (a) Coupon dimension, and (b) Strain gauges configuration (reproduced from ASTM D5379-19 [2019] – all dimension in mm)27
Figure 3.3: Coupon specimens, (a) Tension coupons, (b) Compression coupons, and (c) Shear coupons.....28
Figure 3.4: Tension coupon test equipment.....29
Figure 3.5: Compression test fixture.....29
Figure 3.6: Shear test fixture.....30
Figure 3.7: Examples of failure modes for tension coupons, (a) Failure near the center, and (b) Failure near the grip tab.....32
Figure 3.8: An example of failure mode for compression coupons.....34
Figure 3.9: Failure mode for a 2.5-mm thick shear coupon.....36
Figure 3.10: Immersed wood samples.....38
Figure 3.11: Spraying process for small wood samples, (a) Spraying the composites, (b) Rolling the sprayed composites, and (c) Sprayed composites curing.....39
Figure 3.12: Drill the marked specimen.....41
Figure 3.13: Pull-off test setup.....42
Figure 3.14: Bond strengths of all specimens.....42
Figure 3.15: Failure mode - PRF samples.....44
Figure 3.16: Failure mode – HMR sample (H-W-10-0).....45
Figure 3.17: Failure mode – sample without adhesive.....46

Figure 3.18: Confinement test setup 48
Figure 3.19: Examples of failure mode, (a) N-0, (b) H-0, (c) N-4, (d) H-4, (e) N-6, and (f) H-10 50
Figure 3.20: Stress-strain relationship of the sprayed normal-strength concrete cylinders 52
Figure 3.21: Stress-strain relationship of the sprayed high-strength concrete cylinders 52
Figure 4.1: Details of isolated pole specimens, (a) Actual pole in the field, and (b) Isolated pole specimen in the lab (dimensions in mm) 56
Figure 4.2 : Schematic of Series II poles, (a) Specimens O-4LP-6-S and O-4LP-8-S, and (b) Specimens O-3LP-4-L and O-3LP-6-L (Dimensions in mm) 59
Figure 4.3: Schematic of Series III poles, (a) Specimen N-3RP-0-T, (b) Specimen N-3RP-6-T, (c) Specimen N-3RP-6-C, (d) Specimen N-3WC-0-TB, and (e) Specimen N-3WC-6-TB (Dimensions in mm) 60
Figure 4.4: Details of NSM-GFRP bars layout 61
Figure 4.5: Spraying process: (a) Pole setup, (b) GFRP spraying, (c) Rolling the sprayed composite, and (d) Sprayed composite left to cure 62
Figure 4.6: Side view of the test setup (top part) during a test 63
Figure 4.7: Schematic drawing of the test setup, (a) Side view, and (b) Plan view 64
Figure 4.8: Concrete base in the laboratory 65
Figure 4.9: Details of fillers between the pole and base (Dimensions in mm) 66
Figure 4.10: Data Acquisition System 67
Figure 4.11: Load-deflection relationship at loading point – Series I: control poles 70
Figure 4.12: Typical failure mode for control poles (pole N-3WC-0-X) 71
Figure 4.13: Load-deflection relationship at loading point – Class-4 Series II poles 73
Figure 4.14: Load-deflection relationship at loading point – Class-3 Series II and control pole 73
Figure 4.15: Failure modes – Series II poles, (a) Specimen O-4LP-6-S, and (b) Specimen O-3LP-4-L 74
Figure 4.16: Load-deflection relationship at loading point – Class-3 RP Series III and control pole 77

Figure 4.17: Load-deflection relationship at loading point – Class-3 WC Series III and control pole 77
Figure 4.18: Failure modes – Series III poles, (a) Specimen N-3RP-0-T, (b) Specimen N-3WC-0-TB, (c) Specimen N-3RP-6-C, and (d) Specimen N-3WC-6-TB 79
Figure 4.19: Details at groove after the test – specimen N-3RP-6-T 80
Figure 4.20: Epoxy conditions after the test for specimen N-3WC-6-TB, (a) De-bonded epoxy, and (b) Epoxy cracks 81
Figure 4.21: Load strain relationship for all NSM GFRP bars on specimen N-3WC-0-TB 84
Figure 4.22: Load-strain relationship for all NSM GFRP bars on specimen N-3WC-6-TB 84

LIST OF NOTATIONS

A	=	average cross-sectional area of coupon, mm^2
A_n	=	average cross-sectional area of coupon across the notch, mm^2.
C	=	circumference of the pole at the groundline or failure section, mm
C_N	=	circumference of the pole at the notched section, mm
D	=	diameter of the loading fixture/diameter of the pole at groundline section, mm
d_b	=	diameter of the GFRP bars, mm
E^{chord}	=	tensile/ compressive chord modulus of elasticity, MPa
F	=	maximum fibre stress for the pole at groundline or failure section, MPa
$F_{modified}$	=	modified load requirements, kN
$F_{original}$	=	original horizontal load requirements from CSA O15-15 (CSA 2019), kN
F_P	=	the pull-off force; kN
F_{tu}	=	ultimate tensile strength, MPa
F_u	=	ultimate shear strength, MPa
$f_{u,FRP}$	=	ultimate tensile strength of the sprayed FRP coupons, MPa
G^{chord}	=	shear chord modulus of elasticity, MPa
h	=	height of the groundline, which is 1,220 mm in this study, mm
L_{cut}	=	cut pole length, mm
$L_{original}$	=	original pole length, mm
P	=	lateral load capacity of the pole, kN
P_{est}	=	estimated load capacity of the pole, kN

P_{exp}	=	experimental failure load for the pole, kN
P_f	=	factored lateral load to applied on the retrofitted pole, kN
P_{FRP}	=	lateral load capacity of the sprayed GFRP layer, kN
P_o	=	lateral load capacity assuming a new pole, kN
P_N	=	load capacity of the pole at the notched section, kN
$P_{N,FRP}$	=	lateral load capacity of the sprayed GFRP layer at the notched section, kN
P_i	=	force at the ith data point, kN
P_{max}	=	maximum force before failure, kN
P_u	=	the lower of ultimate or force at 5% engineering shear strain, kN
R	=	radius of the pole at the groundline section, mm
R_N	=	radius of the pole at the notched section, mm
t_{FRP}	=	thickness of the sprayed GFRP layer, mm
γ^a	=	ultimate engineering shear strain, με
γ_i	=	engineering shear strain at ith data point, με
Δ_L	=	longitudinal deflection of the load point at the maximum load, mm
$\Delta\gamma$	=	difference between the two strain points, which is 0.004
$\Delta\tau$	=	difference in applied shear stress between two strain points, MPa
$\Delta\varepsilon$	=	difference between the two strain points, which is 0.002
$\Delta\sigma$	=	difference in applied tensile/ compressive stress between 1,000 and 3,000 με, MPa
ϕ_{FRP}	=	material resistance factor of the sprayed FRP
τ_i	=	shear stress at the ith data point, MPa
ε_{+45}	=	+ 45° normal strain at the ith data point, με

ε_{-45}	=	- 45° normal strain at the ith data point, με
ε_b	=	strain from the back gauge, με
ε_f	=	strain from the front gauge, με
σ_i	=	tensile stress at the ith data point, MPa
$\sigma_i{}^c$	=	compressive stress at the ith data point, MPa
σ_P	=	pull-off bond strength, MPa

CHAPTER 1 – INTRODUCTION

1.1 Background

As the support of overhead line conductors, utility poles play an important role in electricity supply. In addition to precast concrete poles and steel towers, wooden poles are the most common type of utility support at present because of their sustainability, accessibility, excellent nonconducting properties, and construction flexibility (Lines et al. 2019). According to the North American Wood Pole Council (NAWPC 2021), there are approximately 150 million wooden utility poles in North America. Wooden utility poles are usually selected so that they could carry the applied loads, which include wind loads due to the wind pressure on the pole and that transmitted by the cables, in addition to the self weight of the cables, crossarms and any other attachments. Wooden poles are assumed to carry the aforementioned loads as a cantilever beam, for which the poles may be recognized by their horizontal load carrying capacity.

To achieve the maximum economic efficiency possible, utility companies focus on ensuring that the existing poles can be utilized to their full potential. On average, wooden poles need to be replaced at an approximate age of 40 years (Datla and Pandey 2006). However, many internal and external factors can shorten the service life of wooden poles. The internal factors may include the characteristics of the wooden pole, wood treatment quality, exposure conditions and maintenance (Morrell 2016). On the other hand, external factors such as traffic accidents, environmental degradation, decay, and damage caused by humans and woodpeckers, will also reduce the service life of wooden poles (Gezer et al. 2015). Amongst those, environmental deterioration and decay are the main and inevitable problems for most wooden

poles. Preservatives were used to extend the service life of wooden poles by improving the resistance to degradation or decay (Bolin and Smith 2011). Nonetheless, these materials can only slow down the decay process to a certain extent.

In general, replacement of the entire pole is required when it is severely damaged, new upgrades in design guidelines are introduced, or when there are adjustments to the electricity transmission lines. According to a report by Manitoba Hydro (Manitoba Hydro 2012), there are approximately 5,000 new wooden poles used in replacement annually with an average replacement cost of $3,500 for each pole. This high replacement cost will result in an approximately $350 million investment deficit by the year 2032. Therefore, new cost-effective alternatives are required to lower the replacement rate of wooden poles by restoring their load-carrying capacity and thereby extending their service life.

For most wooden poles, rehabilitation and partial replacement are the common methods used to extend the service life. However, the economic benefit of rehabilitation is much greater than that of replacement, not only because of the costs of the new pole sections, transportation, and labour, but also since most of the preservatives used for wooden poles treatment are hazardous, which requires a specialized disposal process for the replaced poles. From an environmental benefit point of view, rehabilitation can also considerably reduce wood consumption, which makes it the most economical option for extending the service life of wooden utility poles.

In most cases, degradation usually occurs within the range of 460 mm above and below the ground line (Hays 1986), which usually causes wooden poles to fail near the groundline section. Therefore, different methods have been introduced to rehabilitate this area to restore or even improve the load-carrying capacity of wooden poles. The most popular rehabilitation method

is using steel trusses, which are attached and secured alongside the wood pole to transfer the horizontal loads to the ground, bypassing the decay zone near the ground line (Gardner 2012). However, even though some steel trusses can be galvanized to reduce the possibility of corrosion, the steel itself may still be vulnerable to corrosion in the long term. Therefore, the non-corrosive fibre-reinforced polymer (FRP) was proposed for wooden pole rehabilitation. The use of externally bonded (EB) FRP laminates to rehabilitate wood pole started in the 1970s, and it has become more and more popular in recent years due to its prominent performance. Previous research found that retrofitting using EB-FRP composites is a cost-effective approach that can successfully restore the load-carrying capacity of the damaged wood poles almost up to its original capacity (Lopez-Anido et al. 2003; Polyzios and Kell 2007; Saafi and Asa 2010). Nevertheless, with the continuous progress and advancement in polymer science, more research is required to better understand the performance of wood poles repaired using FRP materials.

In the last two decades, sprayed-FRP composites have been used in structural rehabilitation and strengthening of reinforced concrete (RC) structures in the regions where EB-FRP wrapping was not possible (e.g., beam-column joints). Ease of application of sprayed-FRP was also reported in addition to having less susceptibility to debonding (Boyd 2000; Yang et al. 2016). Previous research demonstrated that the sprayed-glass FRP (GFRP) can provide better enhancement of ultimate load capacity and energy absorption compared to those provided by EB-FRP for bridge girders (Banthia et al. 2002). Overall, the use of sprayed-FRP to retrofit RC and masonry structures is considered a promising and cost-effective method that can increase strength, stiffness, and energy absorption capacities under different loading schemes including

seismic (Parghi and Alam 2018; Mohit and El-Salakawy 2019). Despite the promising results of sprayed-FRP technique, no research data is available on wood pole rehabilitation using it, and, hence, no design guidelines for using sprayed-FRP in wood pole rehabilitation are available.

On the other hand, retrofitting using near-surface mounted (NSM) bars is a well-established retrofitting technique for concrete and timber structures (El-Salakawy and Islam 2014; Bakalarz et al. 2020; Yeboah and Gkantou 2021). The NSM-GFRP bars could be a promising technique for wood pole rehabilitation, therefore, this study also evaluates the feasibility and efficiency of NSM-GFRP bars compared to the sprayed-GFRP technique.

1.2 Research Significance

This study evaluates the feasibility of using and performance of sprayed-GFRP composites and/or NSM-GFRP bars to rehabilitate wooden poles. The proposed technique provides a structurally efficient and cost-effective rehabilitation option that addresses and resolves the current problems in the utility wood pole industry, such as increasing costs of the pole replacement and disposal of the decommissioned ones. In addition, sprayed-GFRP has higher potential compared to EB-FRP technique, due to the better compatibility, efficiency, and versatility of the former. Furthermore, this study provides experimental and analytical data on the use of sprayed-GFRP for wooden poles retrofitting, which could serve as a basis for design guidelines for such retrofitting method.

1.3 Research Objectives

The main objective of this research is to evaluate the feasibility and performance of sprayed-GFRP composites and/or NSM-GFRP bars in the rehabilitation of wooden utility poles. This

main objective is achieved through the following specific objectives:

- Determining the tensile, compressive and shear properties of sprayed-GFRP composites, which was achieved through coupon tests.
- Evaluating the bond performance between the poles and the sprayed-GFRP composites, with and without adhesive in between.
- Evaluating the confinement performance of the sprayed-GFRP composites.
- Determining the feasibility of using sprayed-GFRP composites, with different thickness and spraying lengths, in rehabilitating decommissioned wooden utility poles.
- Evaluating the efficiency of sprayed-GFRP composites in retrofitting partially damaged poles with 50% cross-sectional reduction.
- Evaluating the performance of NSM-GFRP bars, with and without sprayed-GFRP, in repairing partially damaged poles with 50% cross-section reduction.
- Developing an analytical model to predict the load carrying capacity of the retrofitted poles using sprayed-GFRP with reasonable accuracy.

1.4 Scope of Work

This research project focused only on rehabilitating wooden utility poles with a specific sprayed-GFRP composite and/or a specific size (No. 10) of the NSM-GFRP bars. The sprayed-GFRP composite is made from unsaturated polyester resin and glass fibres. In addition to having the least cost, glass fibre composites were chosen due to their favorable properties such as relatively high strain capacity, thermal and electrical non-conductivity, and better impregnation in different types of resins (ACI 2017). The 6.7-m long pole specimens tested in this study were Class-3 Red Pine, Class-3 Western Red Cedar, Class-3 Douglas Fir, and Class-

3 and -4 Lodgepole Pines, which were cut from 12,192-mm long, full-scale utility poles. Furthermore, the sprayed-GFRP composite was used to retrofit two types of poles: (1) old poles removed from distribution lines, and (2) poles that have a 50% cross-section reduction. The results of this study might not accurately reflect the performance of sprayed-GFRP in rehabilitating wooden utility poles with other classes, species, and/or damage types.

1.5 Methodology

Two phases comprised this research project; material tests for sprayed-GFRP composites and wooden poles tests. The first phase involved the preparation and testing of small sized sprayed-GFRP specimens, which included coupon tests, pull-off tests, and confinement tests. For coupon tests, all specimens were prepared by hand lay-up spraying on a relatively large surface within a pre-set formwork followed by cutting out coupons to the required dimensions according to the respective ASTM standard. For pull-off and confinement tests, the specimens were produced by spraying GFRP composites on existing wooden pole pieces and concrete cylinders, respectively.

The second phase involved preparing the experimental test setup to test twelve wooden pole specimens, including cutting full-scale wooden poles to appropriate length for laboratory conditions in addition to the construction of a concrete base to confine the pole specimens during testing. All poles were cut to a length of 6.71 m (22 ft), where three poles were tested as control poles while the remaining nine poles were retrofitted with sprayed-GFRP composites and/or NSM-GFRP bars.

1.6 Thesis layout

The thesis consists of 6 chapters as outlined below:

- Chapter 1 provides a general background on this research study, including the problem definition, the current existing methods, and the research significance. Additionally, it also outlines the objectives of this research, the scope of work, the methodology used in this study, and the layout of this thesis.
- Chapter 2 presents the literature review of this study, including existing wood pole rehabilitation techniques, FRP in the rehabilitation of wooden beams and poles, and an introduction of the sprayed-FRP techniques and its applications. This chapter also identifies the test parameters of this study, including sprayed-GFRP coating thickness and coating length, and bond adhesives.
- Chapter 3 discusses the details and results of Phase I of this research project, which includes the material tests for the sprayed-GFRP composites. Phase I included coupon tests, pull-off tests, and confinement tests. For each type of tests, it provides the details of test specimens, test set-up and procedure, test results and discussions.
- Chapter 4 discusses the details and results of Phase II of this research project, which is wood poles tests. This included test method, specimen details, test set-up, instrumentation, test results and discussion.
- Chapter 5 provides a simple analytical procedure to estimate the load-carrying capacity and predict the failure mode and location of retrofitted poles. A simplified equation was also developed therein to calculate the required thickness of the sprayed GFRP coating.
- Chapter 6 summarizes the conclusions of this research project including both Phase I and Phase II. Additionally, it also provides some recommendations and research directions for future work.

CHAPTER 2 – LITERATURE REVIEW

2.1 General

The excessive cutting of trees by humans in the past, coupled with the impacts of environmental change, has led to continuous and serious deforestation around the world. Although many countries have put forward plans to limit or even reverse deforestation, the human demand for wood is still tremendous. Therefore, reducing wood consumption became a major concern. From this point of view, extending the service life of existing wood structures by rehabilitation will make a significant contribution towards reducing the wood demand.

Several products and methods have been used to rehabilitate wooden utility poles. Since the primary concern in civil engineering is always the cost, most rehabilitation products were made of steel or concrete. On the other hand, fibre-reinforced polymer (FRP) has not been used extensively in structural retrofitting due to its relatively high upfront cost, low stock, and lack of universal design guidelines. However, with its continuous development, reduced costs and rising popularity nowadays, using FRP in structural rehabilitation became the most cost-effective option, especially when considering the life-cycle cost.

Many studies have been carried out on repairing and strengthening concrete structures using FRP composites. Nevertheless, only few studies have been carried out on evaluating the performance of the sprayed-FRP technique in structural retrofitting. The following sections cover the aforementioned aspect in addition to the existing wood rehabilitation.

2.2 Wood Rehabilitation

2.2.1 Existing rehabilitation techniques for wooden poles

Osmose (2022) offers a few solutions to extend the service life of wood poles. The most common product used in wood pole restoration is the Osmo-C-Truss as shown in Figure 2.1 (a), which was first developed in 1965, and some of them are still in service now. In this system, a C-shaped steel truss is driven into the ground beside the target wood pole, then the steel truss and the pole are tightly strapped together by using hot-dip galvanized steel straps to provide long-term corrosion resistance. The steel truss is formed from 552-MPa yield strength steel and has four sizes with different ultimate strengths.

(a) (b) (c)

Figure 2.1: Osmose products, (a) Osmo-C-Truss, (b) Osmo-C2-Truss, and (c) FiberWrap^{TM} II (Osmose 2022)

Another similar system is the Osmo-C2-Truss as shown in Figure 2.1 (b). It has the same installation process as the C-Truss system but uses higher yield strength steel (690MPa), which results in lower weight and cost. The special W-shaped steel truss allows this system to minimize the truss rotation. It also has four different sizes with different ultimate strengths.

Combinations of trusses can be used depending on the pole conditions. Osmose (2020) also offered a composite product called FiberWrap™ II as shown in Figure 2.1 (c), which is a composite material with outstanding strength and durability that can be used under extreme weather. The composite material is applied near the ground line of the pole, where decay is the main issue. It is ideal for poles with limited access and poles with overhead limitations that affect the installation process for steel trusses.

Laminated Wood Systems Inc. (2013) also offers a system that is called the PhaseRaiser® system as shown in Figure 2.2 (a), which is used to raise the existing wood pole (up to 20 ft) while keeping the line in service. This system was mainly used for poles that have an average age of 50+ years with good service conditions. Driving into the ground is not required in this system. The cut line is located at 6.5 ft (2.0 m) from the ground line and two steel members are set on the ground and bolted to the bottom section of the pole. After the steel members are secured, the pole will be completely cut through and lifted to the desired height by using the hydraulic lifting unit and cylinders. The top section of the pole is then bolted to the steel members. The safety caps are installed after lifting and a tar paper cover is placed over the cut surface. Two side shields are then positioned and nailed to seal the empty zone which finishes the installation.

Another system produced by Laminated Wood Systems Inc. (2014) called PRS – Pole Reclassification System® as shown in Figure 2.2 (b), which is used to reinforce and reclassify the existing wooden poles. This system is similar to the Osmo-ET-Truss. However, it can increase pole strength to be three or more classes higher. The installation process involves three steps; (1) a lower steel unit is driven into the ground to a certain depth by using a pull-down

winch and an air hammer, (2) an upper steel unit is placed over the lower unit starting from the ground and secured, and (3) machine bolts will then be used to connect the upper steel unit and the pole.

Another system from Laminated Wood Systems Inc. (2017) called PoleEnforcer® Spliced Reinforcement System (SRS) as shown in Figure 2.2 (c), was used to repair damaged wood poles. This system is similar to the Osmo-C-Truss, while it is installed in two steps. First, a lower steel unit is driven next to the pole and a back splice plate is attached to the lower steel unit. Then the upper steel unit is installed on top of the lower unit and the splice channel is attached and secured using nuts and locknuts. The whole unit will then be driven to the desired depth and wrapped using steel straps above the ground line, while caps are also installed on top of the upper steel unit.

Polywater (2019) also introduced a product by the name of UPR^{TM} Pole Repair, which was used to repair the woodpecker damage and pole-line hardware holes. This product is available in two types; the “PR” version, which is in liquid form that flows around wood block fillers to save material; while the other version is called “NF” (No Flow), which is a quick gelling to prevent leaking or drip out of wood cracks at the bottom of the repairing holes. Both versions have the same installation procedure. First debris and water are removed from the hole and the hole is wrapped by using the stretch wrap, then the product is injected into the hole and the injection port is covered by an additional stretch wrap. This product will expand in the hole and fill all the space to create strong adhesion to the wood grain.

(a) (b) (c)

Figure 2.2: Laminated Wood Systems products, (a) PhaseRaiser® system, (b) PRS – Pole Reclassification System®, and (c) PoleEnforcer® Spliced Reinforcement System (SRS)

2.2.2 Fibre-reinforced polymer for rehabilitation of wood members

Plevris and Triantafillou (1992) investigated the mechanical performance of timber beams and columns by applying externally bonded thin Carbon FRP (CFRP) sheets at the tension zone. All wood beams were tested under three-point bending, while all the columns were tested under eccentric axial loading. The test results demonstrated that the use of thin FRP sheets in reinforcing the tension zones of wood members successfully increased the strength, stiffness, and ductility characteristics of the wood members.

Gentile (2000) determined the feasibility of using near-surface mounted (NSM) glass FRP (GFRP) bars in strengthening the flexural strength of sawn timber bridge beams. A total of twenty-six Douglas Fir beams and stringers were prepared as specimens which included twenty-two half-scale beams and four full-scale stringers. Seven half-scale beams and one full-scale stringer were tested as control specimens, whereas the remaining specimens were

retrofitted by the NSM-GFRP bars with three different reinforcement ratios and tested to failure. The test results showed that GFRP-reinforced wood beams had 64% more ultimate tensile strain compared to the control specimens. It was also concluded that the NSM-GFRP bars can effectively prevent crack opening, confine local rupture, and bridge local defects in the timber, increasing the load-carrying capacity of the elements.

Johns and Lacroix (2000) evaluated the performance of different types of FRP sheets in reinforcing timber beams subjected to monotonic loading. Twenty-five pairs of 39 × 89 mm matched samples were cut from the same wood piece to ensure all specimens have similar density, grain, growth patterns, and other characteristics. Specimens were retrofitted on the tension side in three different configurations: 2 layers of 1,000-mm long CF130 carbon fibre, 2 layers of 1,400-mm long CF130 carbon fibre, and 2 layers of 1400mm long U-shaped GFRP straps. The test results showed that the strength of the FRP-retrofitted beams was 40-100% higher compared to the strength of the control beams. Also, the increase in strength and moment resistance was higher than the predicted values from simple transformed section analysis and direct use of Code values for strength. The authors also concluded that local bridging and confining action of the FRP composite on the wood are the reason for the increase in strength.

Considering the outstanding performance of FRP in wooden beam rehabilitation, some researchers had conducted studies on the use of FRP in rehabilitating wooden poles. Kell (2001) investigated the performance of FRP splines in repairing wooden poles. Twenty-seven 3,050-mm long Class 6 jack pine poles were tested by using the cantilever method according to ASTM 1036-99. In the first phase, seven specimens were tested as control specimens to determine the average actual capacity of the wood poles. In the second phase, seven specimens were notched

at 610 mm above the ground line with a 2-mm wide slot halfway through the cross-section. The notches were filled with epoxy and FRP splines, with variable lengths, were installed where the notch coincided with their mid-length. In the third phase, six specimens were tested, two were reinforced with 305-mm long FRP splines and confined using 2 or 4 layers of bidirectional fibre-reinforced tape, two were reinforced with 406-mm long splines and confined using 3 or 4 layers of bi-directional tape, while the remaining two poles were retrofitted using the same previous technique but used a different bonding adhesive. In the last phase, seven poles were prepared using three different reinforcement techniques. The test results showed that wood poles fully rehabilitated by FRP splines exhibited a 67% increase of load-carrying capacity compared to their "at installation" capacity. The author also concluded that adding a confinement layer increased the load-carrying capacity of the FRP-repaired poles.

Lopez-Anido et al. (2003) evaluated the performance of the FRP composite shield system in repairing full-size pre-damaged wood piles. Four 9-m long Southern Yellow Pine, preservative-treated wood piles were tested under three-point bending. Only one wood pile was tested as the reference specimen, while all other three wood piles were notched at 900 mm from the midspan toward the pile tip, reducing about 62% of the cross-sectional area to simulate the damage condition before the test. A notched wood pile was tested as a control specimen, while the other two damaged wood piles were repaired using either cement-based underwater structural grout or shear connectors with an expanding polyurethane non-structural grout. Two cylindrical 3.3-mm thick FRP composite shells, manufactured using the Seemann Composites Resin Infusion Molding Process, SCRIMP^{TM} (TPI 2001), to encase each of the two pre-damaged wood piles. The FRP shell was made from vinyl ester resin, Derakane 411-500 (Dow 1999), with three

layers of unidirectional continuous fabric reinforcement in the longitudinal direction. The primary layer was made of woven E-glass fabric, whereas the two outer layers were made of Chopped Strand Mat (CSM), which were placed on each shell laminate to improve bonding to the substrate and to develop a resin-rich area for environmental protection. The fabricated shells were bonded together by using the underwater curing epoxy adhesive Hydrobond 500 (Superior Polymer 2000), to form the FRP jacket for the wood piles. The test results showed that the moment capacity of the wood pile repaired by the FRP composite shield with cement-based structural grout was much higher than that of the notched control specimen. The authors also concluded that although using the FRP composite shield along with steel shear connectors restored only two-thirds of the moment of the un-notched control pile, this FRP composite shield system can be used for cases where wood damage is not a critical consideration such as marine borer protection.

Saafi and Asa (2010) determined the feasibility of using an in-situ wet-layup FRP in extending the service life of electric distribution and transmission wooden poles. Twenty-seven 30-year-old poles were removed from the service line and divided into 3 groups based on the pole dimensions. Each group had 9 pole specimens with 3 different pre-test conditions; 3 as built, 3 damaged, and 3 damaged-and-repaired. An off-the-shelf wooden filler was used to fill the surface voids on damaged poles which provided a smooth surface for applying the FRP jacket. In addition, Tyfo S fluid epoxy was used as the bonding material for the FRP application process. E-glass Tyfo SHE-51A FRP strip with 1.3 mm thickness and 1.5 m width was used to rehabilitate the damaged poles. A 5-mm thick FRP jacket was applied to the damaged poles at about 1.5D (where D is the pole diameter at the groundline section) above and below the ground

line, with three longitudinal layers and one transverse layer. All specimens were tested horizontal load as a cantilever beam. The test results showed that the FRP jacket restored more than 85% of the original capacity of the wooden poles. The authors also concluded that using FRP jackets to repair the damaged poles can extend their service life for about another 30 years, which makes it a cost-effective method compared to pole replacement.

Merschman et al. (2020) evaluated the effectiveness of FRP jackets in repairing wooden utility poles by considering the climate change impacts. A decay model developed by Wang et al. (2008) was used in this study, and the conclusions from Saafi and Asa (2010) regarding the performance of FRP were used as inputs in the decay model. Poles from three locations, Miami, Charleston, and New York City, were selected as analysis objects in this study. The decay rate of the pole was assumed to be halved after the application of the FRP composite, and the authors also assumed that the strength of FRP does not deteriorate with time. The results showed that the use of FRP in repairing wood utility poles can extend the service life of poles by about 35, 49, and more than 52 years corresponding to the cities mentioned above, respectively.

2.3 Sprayed-FRP Techniques and Applications

2.3.1 Sprayed-FRP systems

The sprayed-FRP composites are made of resin and randomly oriented fibres. The spraying process is conducted by using a spraying machine which consists of a resin tank, spray gun, and pumps. The resin is pumped out from the tank and mixed with the catalyst, then the fibre will be chopped into a certain length in the spray gun and be sprayed on the structures after mixing with the resin and catalyst. A certain fibre-to-resin ratio can also be set within the

spraying machine. As mentioned earlier, the sprayed-FRP system has many advantages compared to the other FRP techniques, which is the reason why more research is being conducted to evaluate the performance of sprayed-FRP.

Yang et al. (2016) analyzed the tensile mechanical properties of sprayed FRP. Three types of fibre; glass, carbon, and basalt, and two types of resin; vinyl ester and unsaturated polyester, were used in that study. A total of 13 groups of specimens with different fibre types, resin types, fibre volume ratios, fibre lengths, and FRP thicknesses were tested to failure, and each group has six specimens. The test results showed that the tensile strength and elastic modulus of the sprayed-FRP with carbon fibres are higher than the ones with glass or basalt fibres. However, the sprayed-CFRP had the lowest strain capacity among all three fibre types. The average tensile strength of sprayed-GFRP using unsaturated polyester resin was about 75.2 MPa. The authors concluded that the tensile performance of sprayed-FRP is always similar to the fibres used. In addition, the vinyl ester resin exhibited better performance compared to the polyester resin in general. On the other hand, the ultimate strain of the sprayed-FRP using polyester resin was larger than the ones use vinyl ester resin when mixed with glass fibres. Moreover, the authors also concluded that every combination of fibres and resin has its optimal fibre volume ratio to obtain the maximum tensile property. The results also showed that an increase in fibre length can improve the tensile performance of the sprayed-FRP composite, whereas the strength decreased when the thickness of FRP layer increased from 4 to 7 mm.

2.3.2 Sprayed-FRP in structural rehabilitation

Boyd (2000) investigated the feasibility of using the sprayed-GFRP technique to retrofit reinforced concrete beams. Results showed that the improvement from the sprayed-GFRP is

similar to the effect of commercially available FRP wraps and plates for flexural strengthening. However, the sprayed-GFRP technique exhibited better performances in terms of shear strengthening. It was also concluded that the strength properties of the sprayed-GFRP can be accurately estimated based on the properties of the resin and fibre that were used in the mix. Besides, the randomly oriented fibres can also increase the resistance to debonding of the sprayed-FRP, which is an immense advantage compared to continuous fibre systems such as FRP wraps and plates. Moreover, the use of the sprayed-GFRP technique can result in significant cost savings by considering the material, labor, and structure downtime costs.

Boyd et al. (2008) evaluated the performance of sprayed-GFRP in repairing prestressed concrete girders. Three 13.3-m long AASHTO Type II girders with 1.2-m deep and 12.2-m test span were used as specimens in this study. Twenty-two prestressing strands were oriented in 3 layers in the bottom portion of each girder. All specimens were tested in flexure until failure. The first girder was tested under the undamaged condition as a control specimen. The remaining two girders were damaged at the center portion over 1,500 mm to expose the prestressing strands, and then the exposed strands were cut to simulate the damages which could cause prestressing strands to rupture. One of the damaged girders was tested without any repair as a damaged control specimen, and the other damaged girder was repaired using sprayed-GFRP before testing. The results showed that the sprayed-GFRP technique can restore the ultimate load-carrying capacity to about 95% of the original capacity of the undamaged control specimen.

Talukdar and Banthia (2010) investigated the performance of sprayed-GFRP in strengthening timber beams. Ten specimens with two different sizes were used; five with 150 × 350 × 2,440

mm and were treated with Boracol (water-based) preservative, while the other five were 150 × 200 × 2,440 mm and were treated with Creosote (oil-based) preservative. Two different bonding agents, AtPrime 2 and Hydroxymethylated Resorcinol (HMR), were used to enhance the bonding between sprayed-GFRP and wood surface. The test results showed that the sprayed-GFRP improved the load-carrying capacity and ductility of the timber beams. In addition, the Creosote-treated beams performed better than the Boracol-treated ones. The results also showed that each type of wood treatment had its preferred bonding agent, which affected the overall performance of the sprayed-GFRP composite.

Hussain and Pimanmas (2015) studied the shear strengthening of RC deep beams with openings using sprayed-GFRP composites. Twenty-nine RC deep beams with different openings and concrete strengths were retrofitted using different sprayed-GFRP configurations and then tested under three-point bending. The test results indicated that the use of sprayed-GFRP in strengthening did remarkably increase the ultimate load and stiffness of the RC deep beams with openings. It was also reported that the ultimate load enhancement increased as the sprayed-GFRP thickness increased.

Lee et al. (2016) investigated the performance of the sprayed-FRP system in strengthening shear-critical RC columns under seismic loading. Five shear-critical columns were constructed where one of them was used as a control specimen, whereas the other four columns were strengthened using four different combinations of glass or carbon fibres and epoxy or vinyl ester resins. All specimens were tested up to failure under lateral cyclic drift reversals. The shear strength of the sprayed-FRP strengthened columns were found to be 31% higher than that of the control specimen. In addition, the strengthened columns exhibited up to 43% larger

lateral deformation compared to the control specimen. The authors also concluded that the sprayed-FRP technique can be used to retrofit the existing low- to medium-rise RC buildings that are not designed according to the seismic specifications.

Mohit and El-Salakawy (2019) investigated the seismic behaviour of splice-deficient RC circular columns rehabilitated with sprayed-GFRP composites. Six large-scale RC columns were constructed and tested under simulated seismic loading before and after rehabilitation. The study included two phases, with three specimens per each. A 3-mm thick sprayed-GFRP layer was used in the first phase, one column was rehabilitated after testing up to 2.5% drift ratio and retested to failure, another column was tested to failure then retested after rehabilitation, and the last column was strengthened before the test. The thickness of the sprayed-GFRP in Phase 2 was increased to 6 mm based on the test results from Phase 1, and the three columns in this phase were also tested under the same conditions as Phase 1. A significant increase in the cumulative energy dissipation capacity was recorded for the columns that were rehabilitated with 6 mm thickness sprayed-GFRP. The test results showed that the use of 6 mm thick sprayed-GFRP can increase the lateral load and the drift capacities of the RC circular column by approximately 12% and 78%over its respective original capacity, respectively. The authors also concluded that the sprayed-GFRP system with an adequate thickness (i.e., 6 mm) can be used to repair even fully damaged columns following a major earthquake.

2.4 Literature Review Summary

Since no research data or design guidelines are available on wood pole rehabilitation using the sprayed-FRP technique, the following preliminary guidelines were determined based on the

literature review discussed earlier. It was decided to conduct this study in two consecutive phases; Phase I which includes the material testing to evaluate the mechanical properties of the sprayed-GFRP composites in addition to its bond and confinement efficiency, and Phase II, in which the pole specimens were planned to be retrofitted based on the conclusions of the first phase.

2.4.1 Sprayed-GFRP coating thickness

As mentioned earlier, many researchers have been using sprayed-GFRP composites to retrofit RC structures. The thicknesses of the sprayed-GFRP composites ranged from 3 to 10.4 mm in the previous research and satisfactory results were obtained. Boyd (2000) concluded that the minimum practical application thickness of sprayed-GFRP composite is 3.5 mm. Moreover, many researchers also concluded that the performance of the sprayed-GFRP composites in rehabilitating or strengthening the concrete structures increases as the GFRP thickness increases. The constraints of using large thickness are always due to the specimen dimensions and the relative cost versus performance improvement.

2.4.2 Sprayed-GFRP coating length

The length of the GFRP coating should be long enough to cover the degradation zone of the wood pole. As demonstrated earlier, the degradation usually occurs within the range of 460 mm above and below the ground line (Hays 1986). Saafi and Asa (2010) did their inspections on the in-service poles and found that the deteriorated area roughly extended to D (where D is the pole diameter at the groundline section) above and below the ground line. In addition, they decided to extend the FRP wrap to $1.5D$ below and above the ground line. Since the average

diameter of the poles used in this project at the groundline section was approximately 320 mm, the distance 1.5*D* would be 480 mm.

2.4.3 Bonding adhesive

Since all wood poles used in this project were treated with waterborne preservative Chromated Copper Arsenate (CCA), a bonding adhesive will be used to improve the bonding performance between wood poles and the sprayed-GFRP composites. Two types of adhesives were tested to evaluate the bonding performance; the first one is a Phenol Resorcinol Formaldehyde resin (PRF) [LRBG Chemicals Inc. 2023], and the other one is Novolak Hydroxy Methylated Resorcinol (n-HMR) [Christiansen and Vick 2000]. The efficiency of those two adhesives was compared to that of the direct application of the composite without any adhesive to determine the best procedure for the pole tests.

CHAPTER 3 - PHASE I: MATERIAL TESTS FOR SPRAYED-GFRP COMPOSITES

3.1 General

Phase I of this project consisted of three different test sets including coupon tests, pull-off tests, and confinement tests. The objective of the coupon tests was to determine the tensile, compressive and shear properties of the sprayed-GFRP composites, so the suitable GFRP coating thickness to be used for the wooden utility poles test could be selected. For pull-off tests, limited portions of the wooden poles were sprayed and tested to evaluate the bond performance between the wood pole and the sprayed-GFRP composites and the adhesives in between, if any. For confinement tests, standard-sized concrete cylinders with different compressive strength were sprayed and tested to evaluate the confinement effects of the sprayed-GFRP composites independently from any complexity associated with the timber poles.

3.2 Materials and Application Procedures

3.2.1 GFRP composites

The GFRP composites used in this study comprised of glass fibres and unsaturated polyester resin, with percentages of the resin and the fibres were 65 and 35%, respectively, which were controlled through the spray gun settings. The spray machine consists of a spray gun with a fibre chopper, that chopped the fibres to a length of approximately 15 mm, a mechanical arm to direct the spray gun, a resin tank, and a pump to direct the resin to the spray gun, as shown in Figure 3.1.

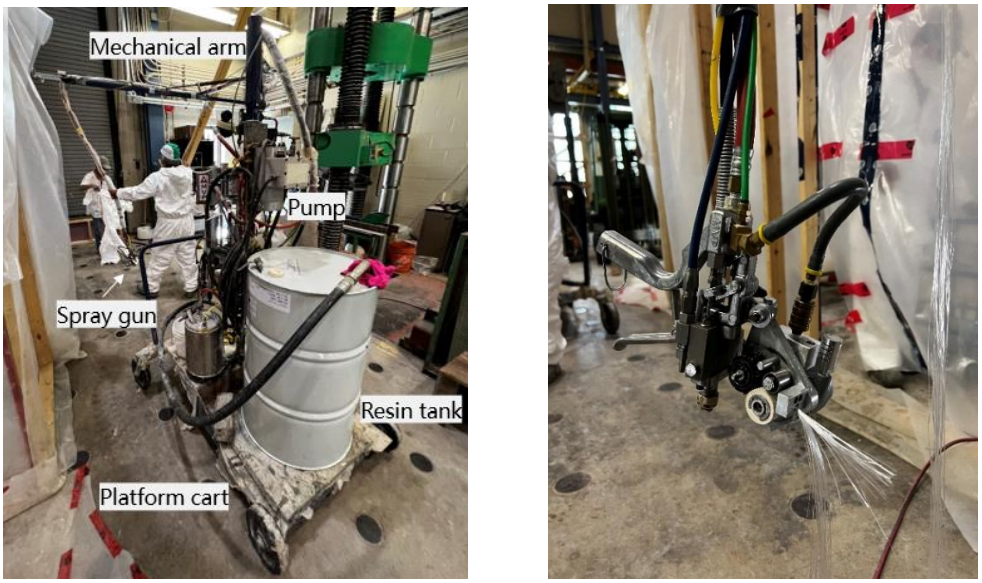

(a) (b)

Figure 3.1: Components of the GFRP spray machine, (a) Spray machine, and (b) Spray gun.

3.2.2 Bonding adhesives

The bonding adhesive included in this phase, as discussed in detail later in Section 3.3, were the Phenol Resorcinol Formaldehyde resin (PRF) [LRBG Chemicals Inc. 2023], and the other one is Novolak Hydroxy Methylated Resorcinol (n-HMR) [Christiansen and Vick 2000]. The manufacturer only provided the ingredients (resin and catalyst) of the PRF (LRBG Chemicals Inc. 2023), since the PRF only has a few hours of working life after mixing the resin and catalyst. According to the test results from LRBG Chemicals, mixing the resin and catalyst in a ratio of 100:20 results in a 30-minute working life and a 1-1.25-hour curing time. However, if the ratio of the mix is 100:15, the working life increases to 1-1.5 hours and the time for full curing will also increase to 5.75 hours. Considering the actual process time in the lab, the initial resin-to-catalyst ratio of 100:20 was used. Since the coating area, PRF application rate, and ingredient ratio were known, the weight of the ingredients was determined. The resin was stirred with an agitator in a cylindrical vessel. Then the well-mixed catalyst slurry was

gradually added to the resin for 1 to 2 minutes. The mix was ready to apply after an additional 4 to 5 minutes of mixing with the agitator. The mix was transferred to a wide tray and rolled on the wooden surface.

The ingredients of n-HMR are summarized in Table 3.1. Since the n-HMR solids content did not impact the bonding, a 5% HMR solids content was used in this project.

Table 3.1: Ingredients of 100 g n-HMR solution

Ingredient	Weight of Chemical (g)
Crystalline Resorcinol	3.34
Deionized Water	90.43
3-Molar Sodium Hydroxide Solution	2.44
Formaldehyde Solution (For Novolak Stage)	0.95
Formaldehyde Solution (For Activation Stage)	2.84
Dodecyl Sodium Sulfate Salt	0.50

The mixing procedure for n-HMR can be divided into two stages. The first stage is the Novolak stage, where the crystalline resorcinol was dissolved in deionized water and the solution was mixed for 5 minutes. Then the 3-molar sodium hydroxide solution was added to the solution and mixed for another 5 minutes. After that, a small amount of the formaldehyde solution was added to the solution and mixed for 5 more minutes. Then the solution was stored before being used. The second stage was the activation stage, where the final portion of the formaldehyde solution was added to the solution and mixed for 5 minutes. Then the pH of the solution was determined after the mixing, where the pH value should be between 8.5 to 9.0. Otherwise, the pH should be adjusted by adding 3-molar sodium hydroxide solution to the n-HMR solution. Once the desired pH is obtained, the solution was allowed to react for one hour. After that, a small amount of dodecyl sodium sulfate salt was added to the solution just before the

application to improve the wetting of the wood surface (Eisenheld 2003). Afterwards, all wood samples were allowed to dry for 18-24 hours under room temperature before spraying the GFRP composite on them.

3.3 Coupon Tests

3.3.1 Test specimens and methods

The sprayed-GFRP tension, compressive and shear coupons were tested in accordance with ASTM D3039-17, ASTM D3410-16 2016, and ASTM D5379-19 2019 (ASTM D3039-17 2017; ASTM D3410-16 2016; ASTM D5379-19 2019), respectively. Table 3.2 summarizes the dimensions of each coupon set in accordance with the test type. Each set included a minimum of 5 samples as required by the respective ASTM standard (ASTM D3039-17 2017; ASTM D3410-16 2016; ASTM D5379-19 2019).

Table 3.2: Dimension details and test type of all sprayed-GFRP coupons

Set	Width (mm)	Length (mm)	Thickness (mm)	Test type
1	25	250	2.5	Tension
2	25	250	6.0	Tension
3	25	250	10.0	Tension
4	10	140	2.5	Compression
5	Figure 3.1 (2.5 mm thickness)			Shear
6	Figure 3.1 (6.0 mm thickness)			Shear

Figure 3.2 (a) shows the dimensions of a shear coupon specimen. The glass fibres were cut to length by the chopper gun, and then sprayed by hand lay-up on a relatively large surface inside a pre-set formwork to ensure achieving the required thickness of the coupons. After the sprayed composite has cured, the coupons were cut out of the obtained large sheet to the required sizes

as shown in Figure 3.3.

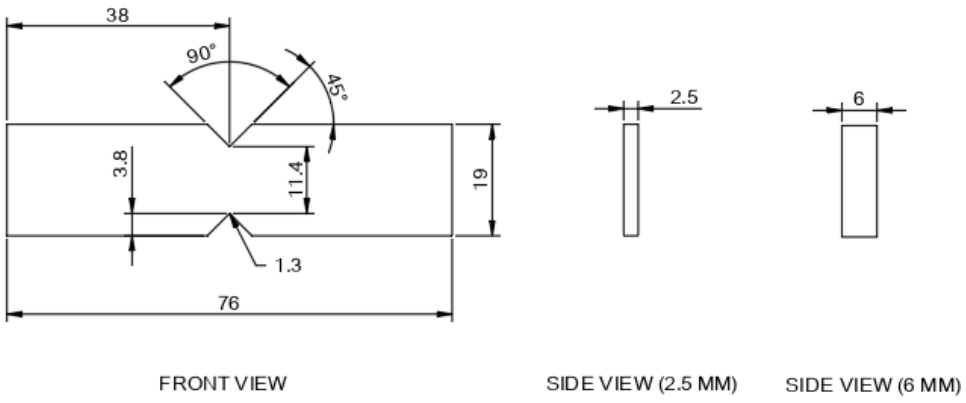

(a)

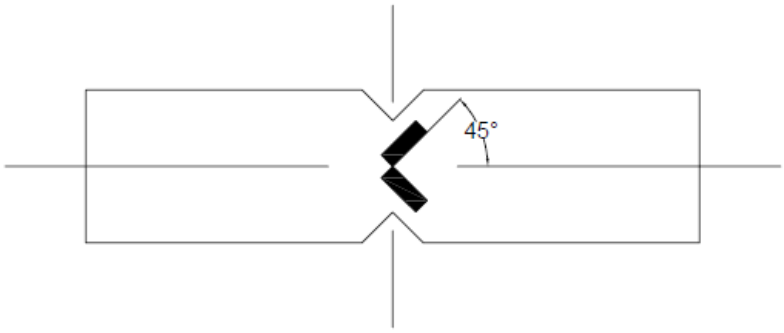

(b)

Figure 3.2: Shear test coupon specimens: (a) Coupon dimension, and (b) Strain gauges configuration (reproduced from ASTM D5379-19 [2019] – all dimension in mm)

Three sets of coupons were tested to determine the tensile properties of sprayed-GFRP composites, where the main variable was the coupon thickness, varied as 2.5, 6.0, or 10.0 mm. Four 2.5-mm thick coupons, cut to the same length of the grip and the same width of the specimen, were bonded on both ends of the specimen using Dural Fast Set Gel (Euclid Chemical 2022). In addition, all compression coupons had a thickness of 2.5 mm, whereas 2.5- and 6-mm thick shear coupons were prepared and tested.

(a) (b) (c)

Figure 3.3: Coupon specimens, (a) Tension coupons, (b) Compression coupons, and (c) Shear coupons

3.3.2 Test setup and instrumentation

A 100-kN capacity testing machine was used to conduct the required tests with different fixtures, as appropriate. For the tension tests, the sprayed GFRP coupons were tested using two heads with a hydraulic wedge grip in each to hold the coupons during the test, as shown in Figure 3.4. A removable fixture having two housing blocks with a movable one along two vertical bearing posts (Figure 3.5) was used to test the compression coupons. Inside each housing block, two wedge grips were used to clamp the coupons. After fixing the coupons, the entire fixture was placed under the loading machine and axial compressive loading was applied through the upper housing block until failure. For the shear test, the V-notched beam test fixture was used, which incorporated two grips and two adjustable jaws that clamp the coupon to ensure no movement or twisting during the test. The lower grip was mounted on the grip holder attached to the bottom baseplate of the testing machine (Figure 3.6), while the upper grip was vertically movable along the bearing post, and the force was applied on the upper grip which

results in the shear force applied to the coupon. A specimen alignment pin was located on the lower grip to make sure the coupon is aligned with the loading axis.

Figure 3.4: Tension coupon test equipment

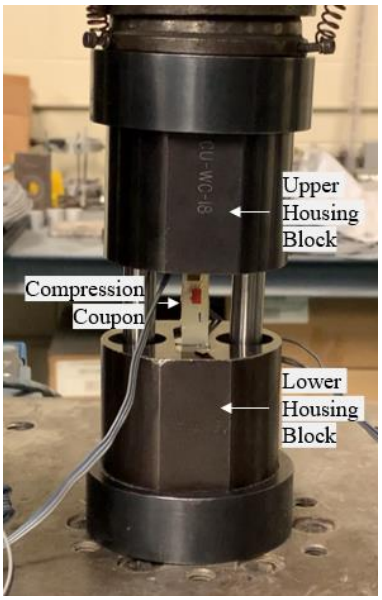

Figure 3.5: Compression test fixture

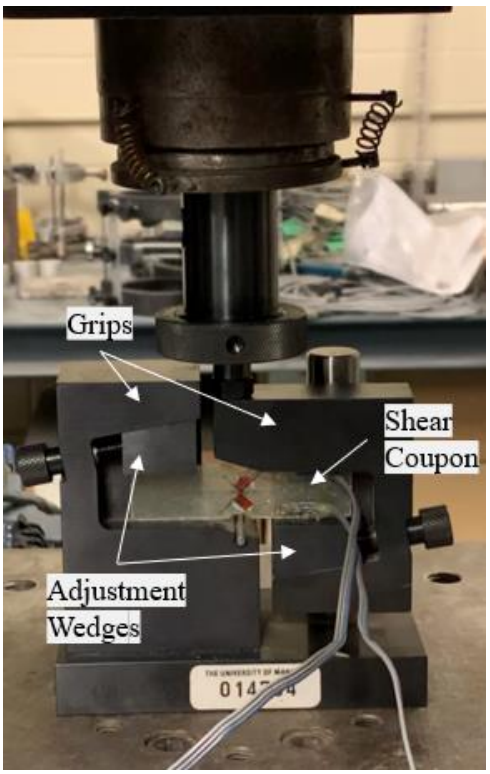

Figure 3.6: Shear test fixture

To measure the strains in the sprayed-GFRP coupons, back-to-back 350-Ω electrical resistance strain gauges with a gage length of 6 mm were installed at the center of the tension and compression coupons. For the shear coupons, two electrical resistance strain gauges were installed at the notched region near the center of the coupons with the specific layout required by ASTM D5379-19 (ASTM D5379-19 2019), as depicted by Figure 3.2 (b).

3.3.3 Test results and discussion

3.3.3.1 Tension coupons

The ultimate tensile strength and tensile stress at any data point were calculated by the following equations:

$$F_{tu} = \frac{P_{max}}{A} \qquad \text{Equation 3.1}$$

$$\sigma_i = \frac{P_i}{A} \qquad \text{Equation 3.2}$$

where:

F_{tu} = ultimate tensile strength, MPa;

P_{max} = maximum force before failure, N;

σ_i = tensile stress at the i^{th} data point, MPa;

P_i = force at the i^{th} data point, N; and

A = average cross-sectional area of coupon, mm^2.

The tensile chord modulus of elasticity was calculated by the following equation:

$$E^{chord} = \frac{\Delta\sigma}{\Delta\varepsilon} \qquad \text{Equation 3.3}$$

where:

E^{chord} = tensile chord modulus of elasticity, MPa;

$\Delta\sigma$ = difference in applied tensile stress between 1,000 and 3,000 με, MPa; and

$\Delta\varepsilon$ = difference between the two strain points, which is 0.002.

Table 3.3 shows the test results of all the tension coupons. The ultimate tensile strength of the sprayed-GFRP coupons increased from 112.7 to 122.0 MPa when the coupon thickness increased from 2.5 to 6 mm. In other words, the coupon gained 8% of tensile strength with a 140% increase of thickness. Furthermore, the increase of tensile strength was 15% when the coupon thickness increased from 6 mm to 10 mm (60% increase in thickness). This indicates a non-linear increase of ultimate tensile strength of the sprayed-GFRP composite as its thickness increases. A similar relationship can also be noticed for tensile chord modulus of elasticity of the sprayed composite. Most of the coupons failed in an explosive manner, where some examples of failure modes are shown in Figure 3.7.

Table 3.3: Test results of tension coupons

Coupon thickness (mm)	Ultimate tensile strength (MPa)	Tensile chord modulus of elasticity (MPa)	Ultimate strain (%)
2.5	112.7 ± 3.3	10,661 ± 246	1.4 ± 0.2
6	122.0 ± 4.2	10,142 ± 295	1.9 ± 0.1
10	139.8 ± 3.1	11,348 ± 117	1.8 ± 0.1

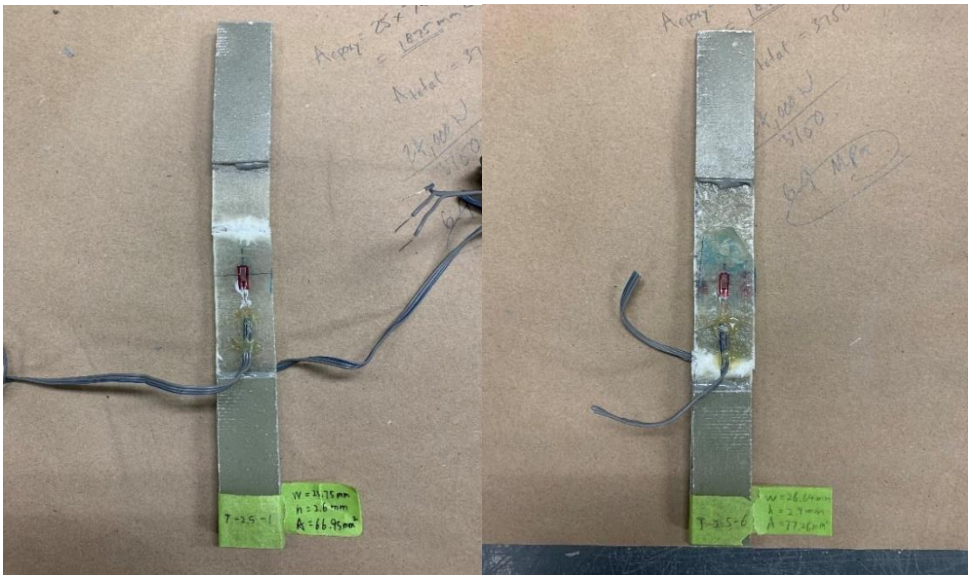

(a) (b)

Figure 3.7: Examples of failure modes for tension coupons, (a) Failure near the center, and (b) Failure near the grip tab.

3.3.3.2 Compression coupons

The ultimate compressive strength and compressive stress at any data point were calculated by the following equations:

$$F_{cu} = \frac{P_{max}}{A} \qquad \text{Equation 3.4}$$

$$\sigma_i{}^c = \frac{P_i}{A} \qquad \text{Equation 3.5}$$

where:

F_{cu} = ultimate compressive strength, MPa;

P_{max} = maximum force before failure, N;

$\sigma_i{}^c$ = compressive stress at the ith data point, MPa;

P_i = force at the ith data point, N; and

A = average cross-sectional area of coupon, mm^2.

The compressive chord modulus of elasticity was calculated by the following equation:

$$E^{chord} = \frac{\Delta\sigma}{\Delta\varepsilon} \qquad \text{Equation 3.6}$$

where:

E^{chord} = compressive chord modulus of elasticity, MPa;

$\Delta\sigma$ = difference in applied compressive stress between 1,000 and 3,000 με, MPa; and

$\Delta\varepsilon$ = difference between the two strain points, which is 0.002.

Due to the limitations associated with the testing fixture, only 2.5-mm thick coupons were tested. Table 3.4 shows the test results of all the compression coupons. The ultimate compressive strength (105.7 MPa) and the compressive chord modulus of elasticity (9,051 MPa) of the GFRP composite were slightly lower compared to its ultimate tensile strength (112.7 MPa) and the tensile chord modulus of elasticity (10,661 MPa). Such test results are promising, particularly for the ultimate compressive strength, considering that the compressive strength of GFRP bars that was reported to be about 50% their tensile strength (Deitz et al. 2003; Tavassoli et al. 2015). This indicates that the multidirectional fibres in the resin gave the sprayed-GFRP composite similar tensile and compressive strengths. All samples failed through thickness near the grip sections or at the gauge spot. Figure 3.8 shows an example of a compression coupon

at failure.

Table 3.4: Test results of compression coupons

Coupon thickness (mm)	Ultimate compressive strength (MPa)	Compressive chord modulus of elasticity (MPa)	Ultimate strain (%)
2.5	105.7 $\pm$ 2.8	9,051 $\pm$ 586	1.3 $\pm$ 0.1

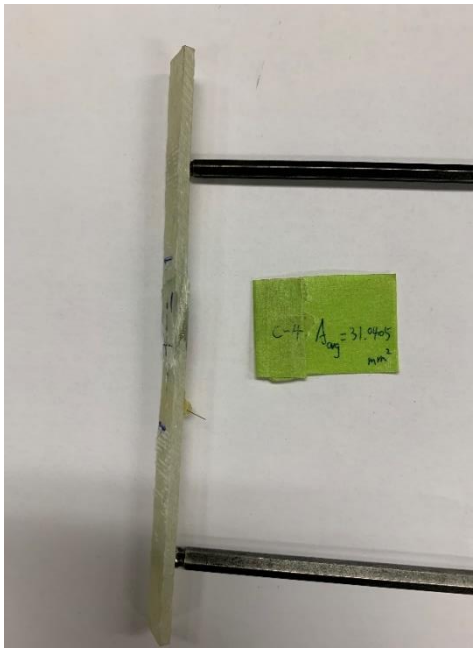

Figure 3.8: An example of failure mode for compression coupons.

3.3.3.3 Shear coupons

The ultimate shear strength and shear stress at any data point were calculated by the following equations:

$$F_u = \frac{P_u}{A_n} \qquad \text{Equation 3.7}$$

$$\tau_i = \frac{P_i}{A_n} \qquad \text{Equation 3.8}$$

where:

F_u = ultimate shear strength, MPa;

P_u = the lower of ultimate or force at 5% engineering shear strain, N;

τ_i = shear stress at the ith data point, MPa; and

P_i = force at the ith data point, N;

A_n = average cross-sectional area of coupon across the notch, mm^2.

The ultimate shear strain and shear strain at any data point were calculated by the following equations:

$$\gamma_i = |\varepsilon_{+45}| + |\varepsilon_{-45}| \quad \text{Equation 3.9}$$

$$\gamma^a = min\begin{cases} 5\% \\ \gamma \ at \ ultimate \ load \end{cases} \quad \text{Equation 3.10}$$

where:

γ_i = engineering shear strain at ith data point, με;

ε_{+45} = + 45° normal strain at the ith data point, με;

ε_{-45} = - 45° normal strain at the ith data point, με;

γ^a = ultimate engineering shear strain, με.

The shear chord modulus of elasticity was calculated by the following equation:

$$G^{chord} = \frac{\Delta\tau}{\Delta\gamma} \quad \text{Equation 3.11}$$

where:

G^{chord} = shear chord modulus of elasticity, MPa;

$\Delta\tau$ = difference in applied shear stress between two strain points, MPa;

$\Delta\gamma$ = difference between the two strain points, which is 0.004.

Table 3.5 shows the test results of the shear coupons. As the coupon thickness increased from 2.5 mm to 6.0 mm, the ultimate shear strength increased significantly from 47.6 to 98.2 MPa.

For samples with 2.5 mm thickness, all samples failed with vertical cracks at the side region, as shown in Figure 3.9, which can be attributed to poor fibre distribution in such small thickness. Therefore, for the rest of Phase I as well as Phase II of this project, it was decided to use a minimum thickness of 4.0 mm to avoid poor fibre distribution that may occur in smaller thicknesses.

Table 3.5: Test results of shear coupons

Coupon thickness (mm)	Ultimate shear strength (MPa)	Shear chord modulus of elasticity (MPa)	Ultimate shear strain (%)
2.5	46.9 $\pm$ 3.5	1,981 $\pm$ 226	3.9 $\pm$ 0.2
6	98.4 $\pm$ 8.4	3,142 $\pm$ 240	3.9 $\pm$ 0.5

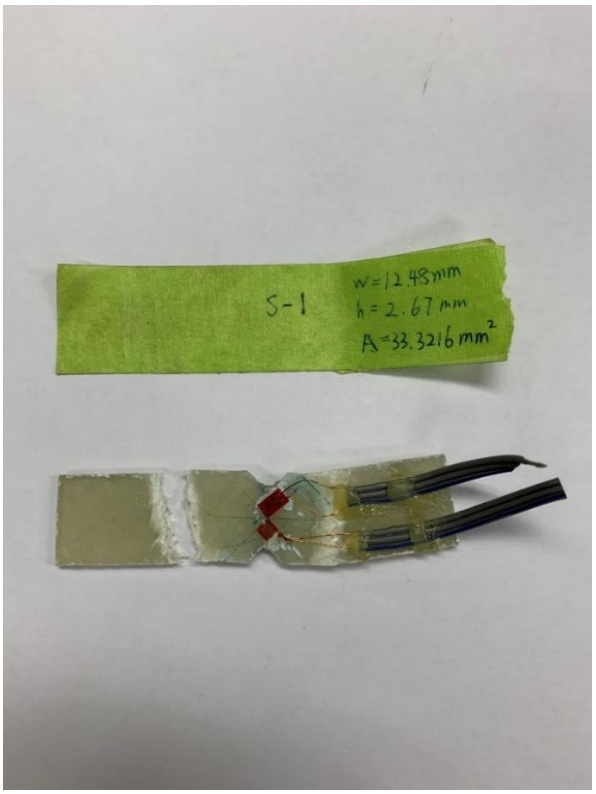

Figure 3.9: Failure mode for a 2.5-mm thick shear coupon

3.4 Pull-off Tests

The second main component in the retrofitting technique to be evaluated was the bond performance between the wooden poles and the sprayed-GFRP composites, with and without

bonding adhesive in between. The objective of this series of tests was to finalize the application process of the sprayed coating including the selected adhesive, if any, to be used in the confinement tests and Phase II of this research project. Tests were performed as per ASTM D7522-21 (ASTM D7522-21 2021), as discussed later in more detail.

3.4.1 Test specimens and methods

Small pieces of new Class-3 Red Pine (RP) wooden poles were prepared for the pull-off test. Each wood sample was approximately 200 mm (8 in.) high with two parallel smooth cuts, near the top and bottom fibres of the cross-section, tangential to the wood grain to create two flat surfaces for the pull-off test. Each specimen was initially planned to be used for five pull-off tests. However, the actual number of tests per wood specimen depended on the surface condition of the sprayed samples. Moreover, the composite was sprayed on some wood specimens in their original air-dried condition, while for the rest of the wood samples a conditioning procedure was applied. This involved immersing the wood samples in a water tank for 7 hours, one day before the spray, followed by air drying overnight for about 17 hours before the spray. Figure 3.10 shows the immersed wood samples in the water tank.

A total of twenty wood samples was prepared and tested. For twelve specimens, the bonding adhesive, the phenol resorcinol formaldehyde (PRF) resin (LRBG Chemicals Inc. 2023) was applied before spraying, whereas the Novolak Hydroxy methylated Resorcinol (n-HMR) adhesive (Christiansen and Vick 2000) was applied on six other specimens. For those specimens, the test variables were the condition of the wood samples before spraying (i.e., dry or wet), the curing time allowed for the adhesive (i.e., 0, 10, 30 or 50 minutes) before spraying the GFRP composite, and the thickness of the GFRP composite (i.e., 6, 8 or 10 mm). It is worth

mentioning that only the specimens prepared using PRF adhesive had the curing time as a parameter, whereas those prepared using n-HMR adhesive were sprayed right after applying the adhesive. The GFRP coating was sprayed on all the sides of the wood samples. Moreover, two wood specimens, a dry and a wet one, were sprayed with the GFRP composite directly without any adhesive, to assess the direct bond performance between the composite and wood. Following the tests on the samples primed with PRF and n-HMR, only the thickness of 6 mm was selected for the GFRP coating for the two specimens sprayed without an adhesive.

Figure 3.10: Immersed wood samples

For the spraying process, a thin layer of resin was sprayed first to enhance the bonding performance between the sprayed-GFRP composites and the wood (or adhesives). After that, the GFRP composites were sprayed around the samples. Small hand rollers were used to achieve a uniform thickness over the sprayed region and force the entrapped air out. Rolling also helped fill the small holes and cracks on the pole surface with the composite. Further

spraying and rolling were repeated until the desired thickness was achieved, which was checked marked pins. Figure 3.11 shows the spraying process for small wood samples.

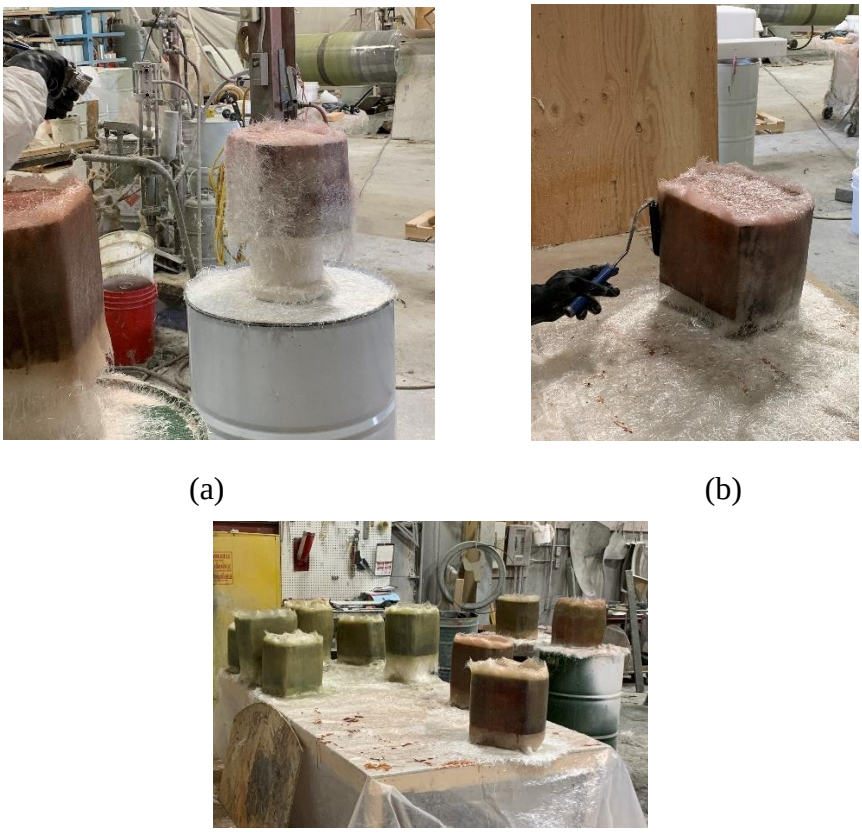

(a) (b)

(c)

Figure 3.11: Spraying process for small wood samples, (a) Spraying the composites, (b) Rolling the sprayed composites, and (c) Sprayed composites curing.

Each set of specimens was designated by a four-character alphanumeric code. The first character represents the adhesive type; P, H, or O for PRF, n-HMR or no adhesive (original), respectively. The second character represents the pole condition; W or D for wet or dry, respectively. The third digit represents the thickness of the sprayed-GFRP layer (i.e., 6, 8 and 10 mm). The last character indicates the curing time of the adhesive (i.e., 0, 10, 30 and 50 minutes, where 0 refers to directly spraying the GFRP coating right after applying the n-HMR adhesive, if any). Table 3.6 summarizes the test matrix for this series of tests.

Table 3.6: Pull-off test matrix and test results

Specimens ID	Adhesive type	Pole condition	Sprayed-GFRP thickness (mm)	Adhesive curing time (min)	**Bond strength (MPa)**
P-D-6-10	PRF	Dry	6	10	0.74 ± 0.3
P-D-6-30				30	0.96 ± 0.6
P-D-6-50				50	1.12 ± 0.6
P-W-6-10		Wet		10	1.24 ± 0.3
P-W-6-30				30	1.70 ± 1.0
P-W-6-50				50	0.99 ± 0.4
P-D-8-10		Dry	8	10	0.81 ± 0.3
P-D-8-30				30	1.57 ± 0.5
P-D-8-50				50	1.29 ± 0.2
P-D-10-30			10	30	0.94 ± 0.3
H-D-6-0	n-HMR	Dry	6	0	1.25 ± 0.2
H-W-6-0		Wet	6	0	1.28 ± 0.2
H-D-8-0		Dry	8	0	0.72 ± 0.2
H-W-8-0		Wet	8	0	0.95 ± 0.2
H-D-10-0		Dry	10	0	0.9 ± 0.2
H-W-10-0		Wet	10	0	1.23 ± 0.1
O-D-6-0	N/A	Dry	6	N/A	1.17 ± 0.4
O-W-6-0	N/A	Wet	6	N/A	1.23 ± 0.2

3.4.2 Test setup and procedure

Since no standards regarding the pull-off test for wood retrofitting systems are available, the ASTM D7522-21 standard for pull-off strength for FRP laminate systems bonded to concrete or masonry was followed (ASTM D7522-21 2021). For each specimen, five flat spots were marked and drilled on one side, as shown in Figure 3.12, or both sides if there were not enough flat spots on one side.

Figure 3.12: Drill the marked specimen.

For each test spot, spherical-headed bolt test fixtures were bonded to the sprayed specimens using Dural Fast Set Gel (Euclid Chemical, 2022). Then each test spot was tested until failure by connecting the test fixture to a pull-off apparatus. Wood shims were used to ensure that the top of the spherical-headed bolt test fixture was levelled, while the apparatus was levelled by adjusting the levelling screws of the apparatus, as shown in Figure 3.13. The failure modes were recorded according to ASTM D7522-21 (ASTM D7522-21 2021), and the pull-off bond strength was calculated using the following equation.

$$\sigma_P = \frac{4F_P}{\pi D^2} \qquad \text{Equation 3.12}$$

where:

σ_P = the pull-off bond strength, MPa;

F_P = the pull-off force, N; and

D = the diameter of the loading fixture, mm.

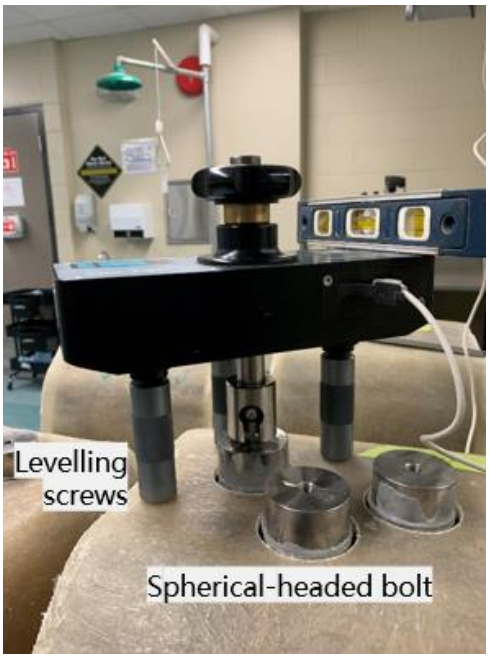

Figure 3.13: Pull-off test setup

3.4.3 Test results and discussion

The pull-off test results are summarized in Table 3.6. Figure 3.14 shows bond strengths of all specimens.

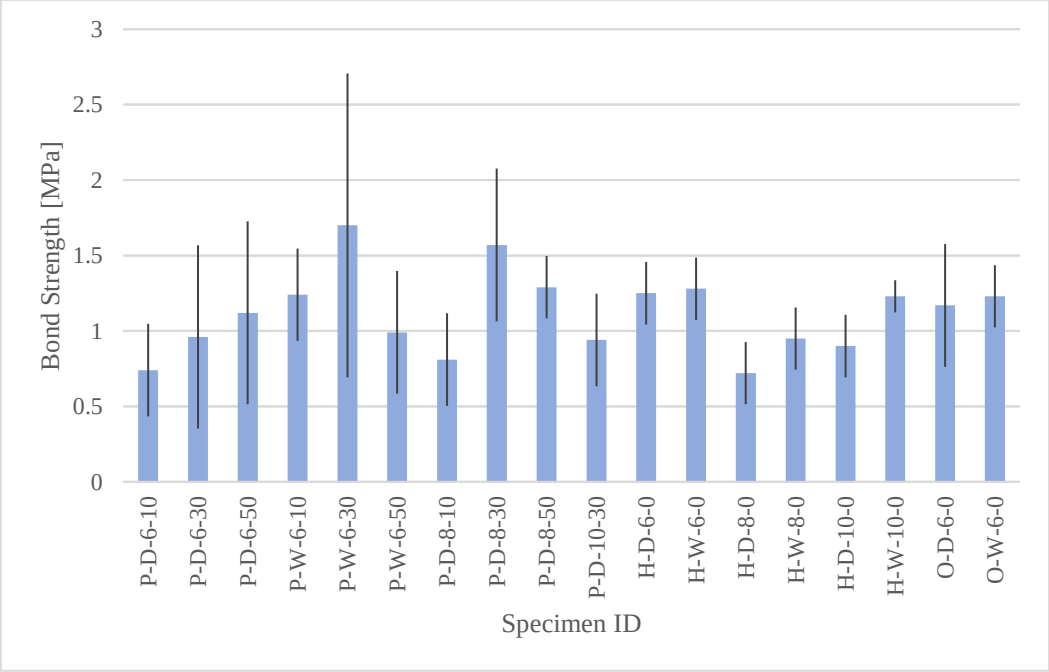

Figure 3.14: Bond strengths of all specimens

Some inconsistencies were observed for the test results, which can be attributed to the variation in the properties of wood at each different spot in addition to the limited control over the thickness of the sprayed composite on such small wood samples. That is, the sprayed resin kept flowing down to the bottom due to gravity before being fully cured. While the same issue also existed during spraying wood poles, better control existed in the latter case since the spraying length was much longer.

3.4.3.1 PRF samples

Generally, the results show that the bond strength was insignificantly affected by the thickness of the GFRP coating, except for when the curing time was 30 minutes, where increasing the thickness from 6 to 8 mm almost doubled the bond strength. In fact, the specimens with an adhesive curing time of 30 minutes exhibited consistently higher bond strength than their counterparts with longer or shorter curing times. An adhesive curing time of 50 minutes resulted in results that were inconsistent with those of the other specimens. Furthermore, the bond strength of the wet samples was mostly higher than that of the dry samples, except for those with a 50-minute curing time.

Figure 3.15 shows the failure remarks of some PRF samples. All the PRF samples failed between the adhesive and the GFRP coating, which indicates that the bonding between PRF and the sprayed-GFRP composites is too weak. This may also justify the large scatter in the results of those specimens. Therefore, PRF was not considered for use on pole specimens in Phase II.

(a) Sample P-D-6-10 (b) Sample P-D-6-50

Figure 3.15: Failure mode - PRF samples

3.4.3.2 HMR samples

No consistent effect could be reported for the sprayed-GFRP coating thickness on the bond strength. In addition, the bond strength of the wet samples was higher than that of the dry samples for sprayed coating thicknesses of 8 and 10 mm, whereas minimal effect could be observed for the sprayed-GFRP thickness of 6 mm.

Although the bond strengths of the HMR samples were mostly similar to those of the PRF samples, the dominant failure mode for the HMR samples was completely different. All HMR samples failed in wood, as shown in Fig. 3.16, which is a desirable mode of failure. This proved that HMR can be used as a primer when spraying GFRP composites on wood poles.

Figure 3.16: Failure mode – HMR sample (H-W-10-0)

3.4.3.3 Samples without adhesive

Since the effects of coating thickness on bond strength are negligible based on the results from PRF samples and HMR samples, lesser original samples were tested. The bond strength was insignificantly affected by specimen conditioning (dry versus wet). The dominant failure mode of all samples without adhesive was the same as the HMR samples, where the samples failed in wood as shown in Figure 3.17. Considering the similar bond strength and failure mode, it was decided, for Phase II of this study, to spray the GFRP composite without priming the pole surface using any type of adhesives.

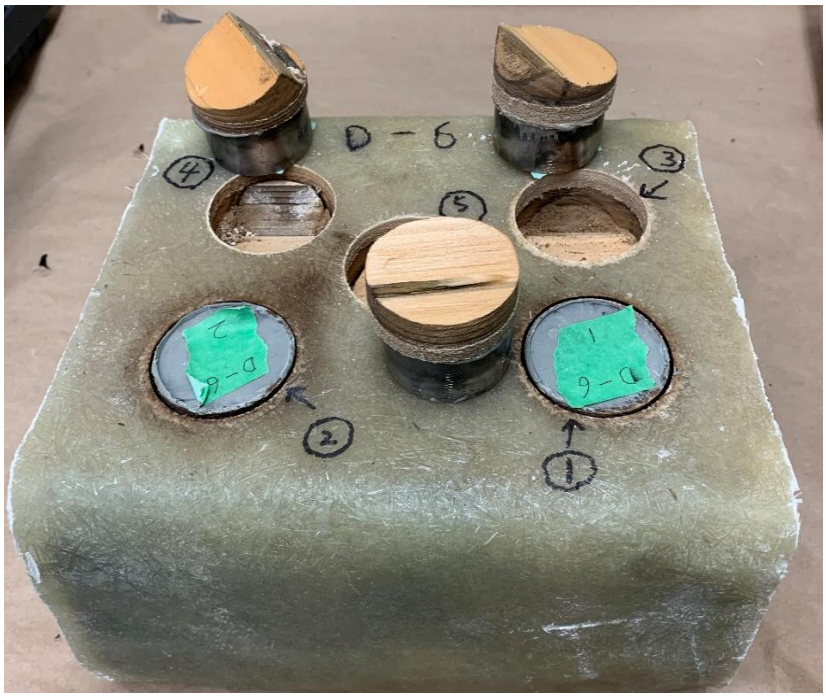

Figure 3.17: Failure mode – sample without adhesive

3.5 Confinement Tests

3.5.1 Test specimens and methods

The objective of this series of tests was to evaluate the confinement efficiency of the sprayed-GFRP composites. To avoid the complexity and potential anomalies associated with testing retrofitted timber replica, ten sets of cylinders were tested; five of which were normal-strength concrete (NSC) with a target compressive strength of 35 MPa, whereas the other five were high-strength concrete (HSC) with a target compressive strength of 70 MPa. All concrete cylinders were 150 × 300 mm. A set of each concrete type was tested without spraying any GFRP composites as a control group, while the remaining sets were strengthened with different thicknesses of sprayed-GFRP before testing. It was much complex to achieve the same thicknesses of 2.5 and 7 mm, used earlier in the coupon tests, while spraying the concrete cylinders. Consequently, thicknesses of 4, 6, 8 and 10 mm were used for the confinement tests.

Based on the test results of the pull-off tests, the GFRP composites were sprayed directly on the concrete sample without prior application of any adhesive on the concrete surface. It is also worth mentioning that the sprayed-GFRP layer was deliberately made slightly shorter than the concrete cylinders at both ends to limit the load transfer to the composites through the hoop (confinement) action. Table 3.7 summarizes the test matrix, where the specimen sets were designated by two characters; the first letter, N or H, represents the concrete strength as normal- or high-strength, respectively; while the second number, 0, 4, 6, 8 or 10, indicates the thickness of the sprayed-GFRP composites in mm (0 denoted control specimens).

Table 3.7: Confinement test matrix

Specimen set ID	Remarks
N-0	Control normal-strength concrete (NSC) cylinders
N-4	NSC cylinders with 4 mm thick sprayed-GFRP composites
N-6	NSC cylinders with 6 mm thick sprayed-GFRP composites
N-8	NSC cylinders with 8 mm thick sprayed-GFRP composites
N–10	NSC cylinders with 10 mm thick sprayed-GFRP composites
H-0	Control high-strength concrete (HSC) cylinders
H-4	HSC cylinders with 4 mm thick sprayed-GFRP composites
H-6	HSC cylinders with 6 mm thick sprayed-GFRP composites
H-8	HSC cylinders with 8 mm thick sprayed-GFRP composites
H-10	HSC cylinders with 10 mm thick sprayed-GFRP composites

3.5.2 Test setup and procedure

Figure 3.18 shows the test setup for the confinement tests. The concrete cylinder was placed on top of a steel base plate that was mounted on a rigid steel base. The concrete cylinder was covered by an acrylic box that was slightly shorter than the concrete cylinder, thereby allowing enough space for the 5000-kN capacity MTS hydraulic testing machine to push the specimen

down. The ultimate load capacity of the cylinders as well as the hoop strain in the sprayed-GFRP layer were recorded through a load cell and electrical strain gauges installed transversally on the surface of the composite, respectively.

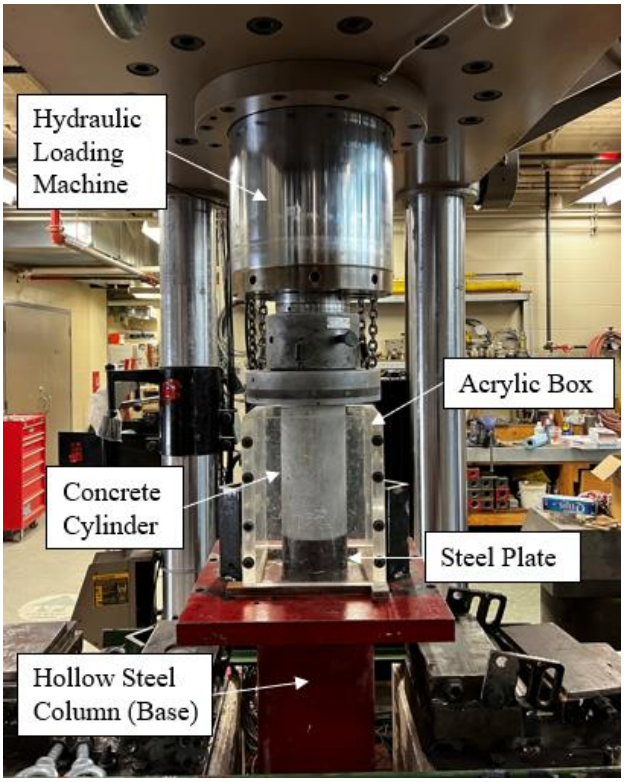

Figure 3.18: Confinement test setup

3.5.3 Test results and discussion

Tables 3.8 and 3.9 show the test results of normal-strength and high-strength concrete cylinders, respectively. For the NSC and HSC cylinders, a 4-mm thick sprayed-GFRP coating increased the compression strength by about 37 and 13% compared to the control set, respectively. However, once the thickness of the sprayed-GFRP coating was increased to 8 mm or above, the compressive strength of the sprayed cylinders significantly increased by around 263 – 318% and 87 – 90% for NSC and HSC sprayed cylinders, respectively. It can be noticed that applying sprayed-GFRP was more beneficial for NSC rather than HSC cylinders. The purpose of this

series of tests was to verify the efficiency of the confinement provided by the sprayed GFRP layer rather than quantifying that confinement stress or effect. The sprayed concrete cylinders exhibited concrete crushing along with rupture of the sprayed-GFRP coating in the hoop direction. Figure 3.19 shows the failure modes of some sprayed concrete cylinders.

Table 3.8: Test results of the normal-strength concrete cylinders

Specimen set ID	Compressive strength (MPa)	Confinement ratio
N-0	31.71	N/A
N-4	43.33	1.37
N-6	127.96	4.04
N-8	115.23	3.63
N-10*	132.45	>=4.18

* The compressive strength is determined excluding the results of the cylinders that did not fail during the tests

Table 3.9: Test results of the high-strength concrete cylinders

Specimen set ID	Compressive strength (MPa)	Confinement ratio
H-0	72.94	N/A
H-4	82.46	1.13
H-6*	137.75	>=1.89
H-8*	138.84	>=1.90
H-10	136.57	1.87

* The compressive strength is determined excluding the results of the cylinders that did not fail during the tests

The confinement ratio was calculated as the ratio of the compressive strength between the sprayed cylinders and the control cylinders. Comparing the confinement ratio of NSC or HSC cylinders with different thicknesses of the sprayed-GFRP layer, the confinement effect increases significantly as the sprayed layer thickness increases from 4 to 6 mm. However,

insignificant increases of confinement ratio can be observed as the thickness of the sprayed coating exceeds 6 mm.

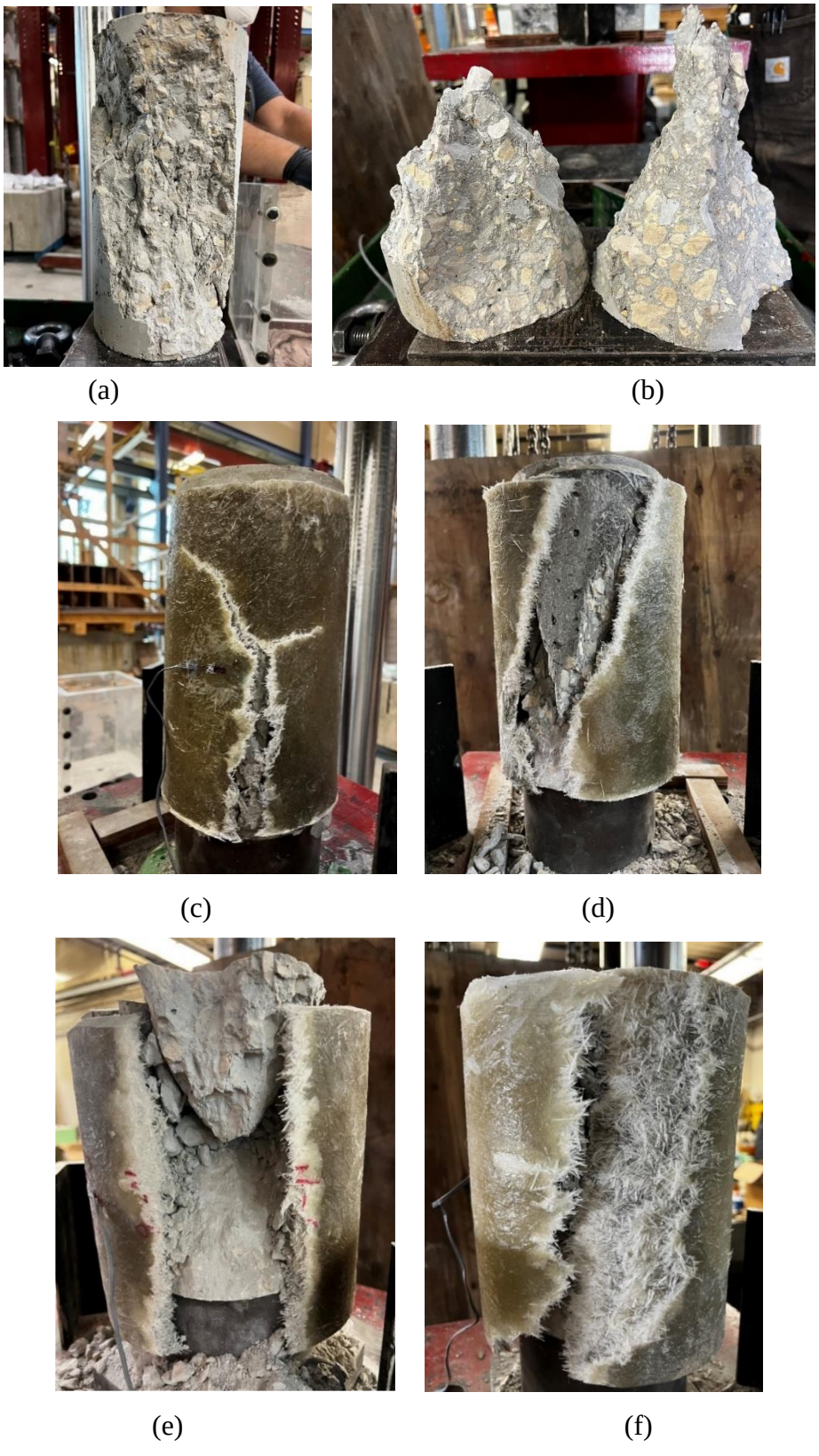

(a) (b) (c) (d) (e) (f)

Figure 3.19: Examples of failure mode, (a) N-0, (b) H-0, (c) N-4, (d) H-4, (e) N-6, and (f) H-10

Based on the previously discussed results, it could be concluded that a 6-mm thick sprayed-GFRP layer would be optimal, as it will provide reasonable tensile strength in the longitudinal and hoop directions, and compressive and shear strengths. Furthermore, increasing the thickness of the GFRP coating may not be beneficial for bonding to the wooden poles or confining them. Nonetheless, it was also deemed imperative to verify the effect of varying the thickness of the sprayed layer on full-scale pole specimens to confirm the material test observations. Chapter 5 summarizes the analytical procedure used to estimate the ultimate load capacity of the poles and the anticipated failure mode and its location.

Figures 3.20 and 3.21 show the relationships of the axial stress on concrete versus the transverse strain in the sprayed GFRP layer for the strengthened NSC and HSC cylinders, respectively. For both types of concrete, it can be observed that the slope of the stress-strain relationship undergoes a remarkable change following the point where the axial stress is approximately equal to the unconfined compressive strength of the control cylinders, which indicates the activation of the sprayed-GFRP confinement afterwards due to the onset of substantial transverse expansion for the concrete cylinders. This was followed by an almost linear response up to failure. It can be also noticed that increasing the thickness of the sprayed-GFRP coating beyond 4 mm resulted in remarkable enhancement in the compressive strength and deformability, whereas there was insignificant effects on the compressive strength and transverse strain as the thickness of the sprayed layer exceeded 6 mm. Figure 3.21 may indicate lower transverse strain values as the thickness of the sprayed-GFRP coating increases, while this can be attributed to the uncertainty associated with concrete where the attached strain gauges on the sprayed layer may be located away from the most stressed section of the cylinders,

which may justify the inconsistencies observed for the recorded transverse strains.

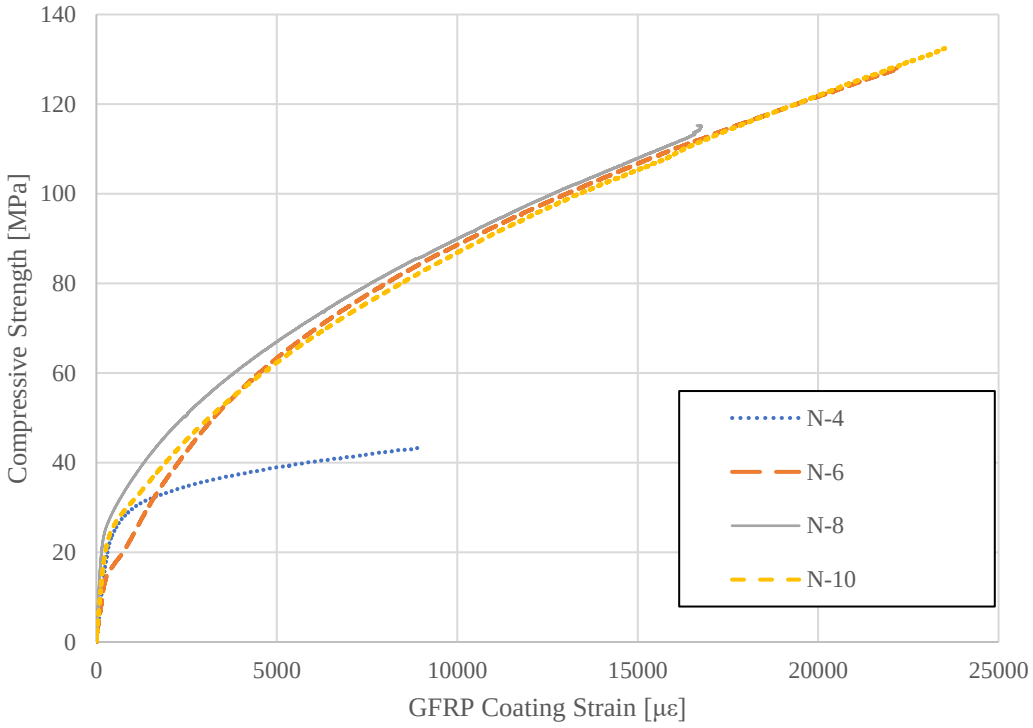

Figure 3.20: Stress-strain relationship of the sprayed normal-strength concrete cylinders

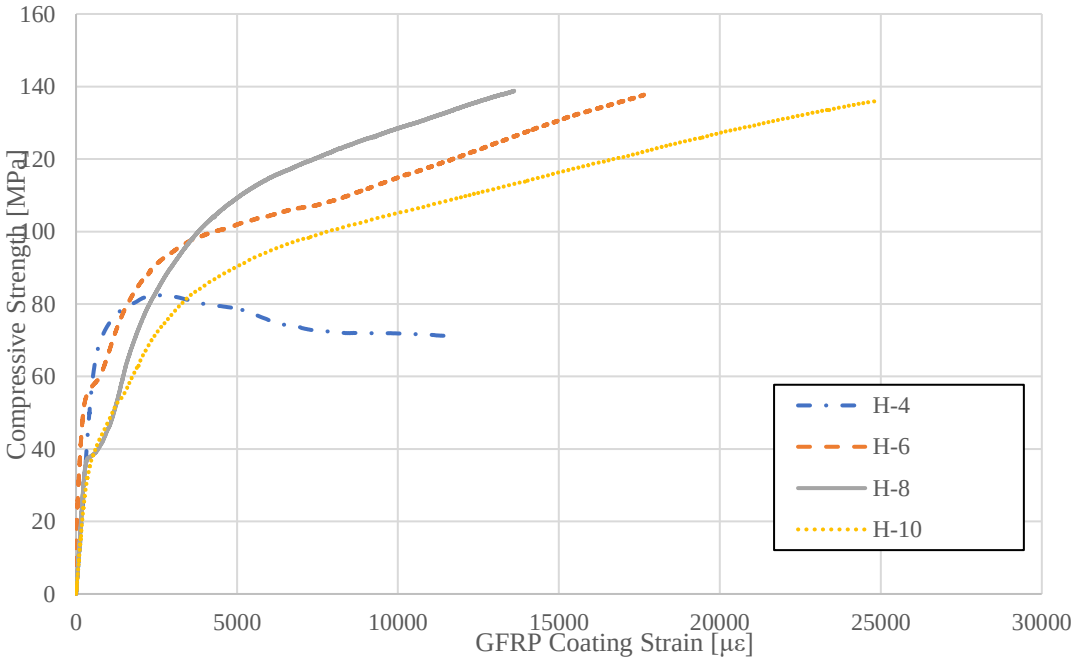

Figure 3.21: Stress-strain relationship of the sprayed high-strength concrete cylinders

CHAPTER 4 - PHASE II: WOOD POLES TESTS

4.1 General

The performance of sprayed-GFRP composites in rehabilitating wooden utility poles under different damaged conditions was evaluated in this phase. In addition, retrofitting using near-surface mounted (NSM) GFRP bars, which is a well-established retrofitting technique for concrete and timber structures (El-Salakawy and Islam 2014; Bakalarz et al. 2020; Yeboah and Gkantou 2021), was used to retrofit the wooden poles to evaluate their feasibility and efficiency compared to the sprayed-GFRP technique. Twelve wooden utility poles were tested in Phase II, three of them were tested as control specimens, and the remaining 9 poles were rehabilitated with sprayed-GFRP and tested under a monotonic horizontal loading up to failure. The test parameters include the thickness (4, 6, and 8 mm) and length (1.0 and 2.0 m) of the sprayed-GFRP coating, and rehabilitation methods (sprayed-GFRP composites, NSM-GFRP bars). The results of the rehabilitated and control poles were compared to evaluate the performance of the sprayed-GFRP composites in rehabilitating wooden utility poles. In addition, the obtained capacities of the rehabilitated poles were compared to the requirement prescribed by CSA O15-15 (2019).

4.2 Materials

A total of twelve full-scale wooden utility poles, including seven air-dried poles with an “at-installation” state (referred to herein as new), whereas the other five poles were decommissioned after full-service life (referred to herein as old). The new poles included Class-3 Red Pines (RP) and Western red Cedar (WC) in accordance with Clause 6.5.3 of CSA

O15-15 (CSA 2019). While old poles were taken from the distribution lines, including Class-3 Douglas Fir (DF), and Class-3 and Class-4 Lodgepole Pines (LP). The CSA O15-15 (CSA 2019) classified the pole based on its length, species, and the circumference at the ground line. Different pole classes have different CSA horizontal load requirements. All wood poles used in this project were treated with waterborne preservative Chromated Copper Arsenate (CCA). Table 4.1 shows the details of wood poles used in this study.

Table 4.1: Wood pole details

Condition	Number of poles tested	Class	Species (species code)
New	4	3	Red Pines (RP)
	3	3	Western Red Cedar (WC)
Old	1	3	Douglas Fir (DF)
	2	3	Lodgepole Pine (LP)
	2	4	

Wood filler was used to fill the notch section of some of the pole specimens (Series III), which will be discussed later. The wood filler used in this study was Pecker Patch (Crosslink Technology Inc. 2002), which is frequently used by Manitoba Hydro. The filler compound consisted of urethane hardener and urethane resin, which was mixed with a one-to-one ratio using a dispensing gun and a mixing tip.

The adhesive used for NSM-GFRP bars was Rotafix Structural Adhesive (Rotafix Northern Ltd. 2023); a two-part adhesive designed for the bonding of timber, masonry, and concrete and consists of epoxy resin and special micro fillers. A silicon compound powder “CAB-O-SIL M5” (Thermo Fisher Scientific UK 2020) was added during the mixing process of the adhesive to produce a thicker yet workable product. The used GFRP bars were No. 10 (9.5-mm diameter)

sand-coated bars with a tensile strength, ultimate tensile strain, and an elastic modulus of 1,376 MPa, 24,000 micro-strains, and 57,333 MPa, respectively, as provided in the certificate of compliance issued by the manufacturer (Pultrall Inc. 2019).

4.3 Specimens Details and Construction Process

4.3.1 Test matrix

A total of twelve full-scale wooden utility poles were tested. The original length of all poles was 12.20 m (40 ft), which typically includes about 1.83-m (6-ft) embedment length below ground line. To accommodate the laboratory and equipment height limitations, the top 4.88 m (16 ft) of the poles were cut off. This height difference required adjustments to the experimental results to be compared against code predictions, as will be discussed later. In addition, the bottommost 610 mm (2 ft) of each pole were removed to enable accessible preparation and rehabilitation for the specimens, while maintaining the location of the ground line. As a result, the height of groundline section, which was represented for lab conditions by the top surface of the concrete supporting block (as discussed later in the test setup section), was about 1.22 m (4 ft) above the lab strong floor, as depicted in Figure 4.1.

The test specimens were divided into three series, I, II and III. The designation of each specimen was a four-character label, where the first letter represents the condition of the wooden pole, either as new “N”, or old “O”. The second character contains a number that represents the class of the pole as per CSA O15-15 (CSA 2019), which was either Class 3 or 4, and two letters that stand for the wood species (CSA 2019) of which the pole specimen was made. The third number identifies the thickness of the sprayed-GFRP coating, which was 0 for

control poles, and 4, 6 or 8 for poles retrofitted with a 4-, 6- or 8-mm thick layer of sprayed GFRP, respectively. The last character of the specimen ID was denoted as "X" for Series I (control) poles, whereas it implied a specific variable for the specimens of series II and III, such as the length of the sprayed region for Series II poles, denoted as "S or L", for the short length of 1.0 m or the longer length of 2.0 m, respectively, as will be discussed in more detail later. For Series III poles, the last character of the specimen ID indicated the location of the notched region, either as "T or C", for notches on tension and compression side of the pole, respectively. Moreover, the incorporation of NSM-GFRP bars as the main or an additional retrofitting technique was indicated by the letter "B" within the last character of the designation of the test specimen.

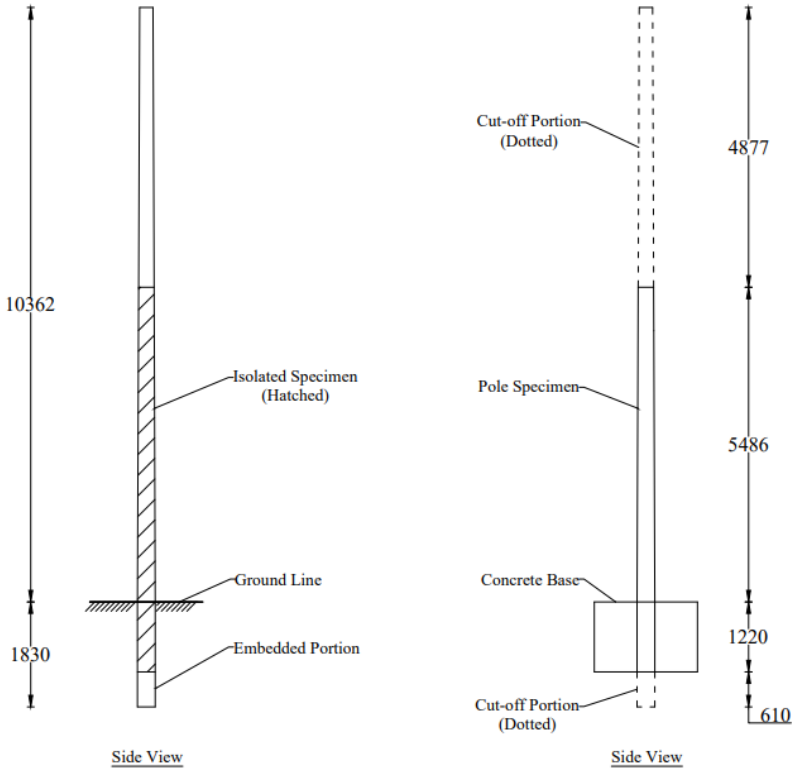

Figure 4.1: Details of isolated pole specimens, (a) Actual pole in the field, and (b) Isolated pole specimen in the lab (dimensions in mm)

For instance, specimen O-4LP-6-S was an old Class 4, Lodgepole Pine pole that was retrofitted using a 6-mm thick layer of sprayed GFRP over a 1.0-m length. Specimen N-3WC-6-TB was a new Class 3, Western red Cedar pole that was notched on the tension side and then rehabilitated using NSM GFRP bars along with a 6-mm thick layer of sprayed GFRP, as discussed later in more detail. Table 4.2 summarizes the test matrix.

Table 4.2: Test matrix

Series	Specimen ID	Condition	Pole class & species	Sprayed-GFRP thickness (mm)	Sprayed-GFRP length (m)
I	N-3RP-0-X	New	3 RP	0	0
	N-3WC-0-X	New	3 WC	0	0
	O-3DF-0-X	Old	3 DF	0	0
II	O-4LP-6-S	Old	4 LP	6	1.0
	O-4LP-8-S	Old	4 LP	8	1.0
	O-3LP-4-L	Old	3 LP	4	2.0
	O-3LP-6-L	Old	3 LP	6	2.0
III	N-3RP-6-T	New	3 RP	6	1.3
	N-3RP-6-C	New	3 RP	6	1.3
	N-3RP-0-T	New	3 RP	0	0
	N-3WC-0-TB	New	3 WC	0	0
	N-3WC-6-TB	New	3 WC	6	1.3

4.3.2 Series I – Control specimens

Series I included two new poles, N-3RP-0-X and N-3WC-0-X, and an old pole O-3DF-0-X were tested as control specimens, while the remaining poles were divided into two series, namely II and III.

4.3.3 Series II

For Series II, which included four old Lodgepole Pine (LP) poles, two poles were retrofitted using 1.0-m (3.3-ft) long sprayed GFRP layer, with a thickness of 6 and 8 mm for specimens O-4LP-6-S and O-4LP-8-S, respectively. The other two old poles were sprayed over a length

of 2.0 m (6.6 ft) with a 4- and 6-mm thick GFRP layer for specimens O-3LP-4-L and O-3LP-6-L, respectively. The purpose of testing this series was to evaluate the efficiency of sprayed GFRP, with varied lengths and thicknesses, restoring the at-installation load-carrying capacity of the poles. It is worth mentioning that all sprayed GFRP layers for Series II poles started approximately 500 mm below the ground line, which can be achieved in practice by removing the embankment around the pole to be retrofitted, to avoid stress concentration at the ground line (Saafi and Asa 2010). This makes the length of the sprayed GFRP layer 0.5 and 1.5 m above the ground line for the specimens retrofitted with the short- (i.e., O-4LP-6-S and O-4LP-8-S) and long-length (i.e., O-3LP-4-L and O-3LP-6-L) sprayed GFRP layers, respectively. The short coating length (i.e., 1.0 m) was determined as the larger of the observed degradation zone by Hays (1986), which usually occurs within the range of 460 mm (1.5 ft) above and below the ground line, and the recommend total length for the retrofitted region of 3.0 times the diameter of the pole (Saafi and Asa 2010). The longer coating length (i.e., 2.0 m) was determined by doubling the previously discussed short length. Figure 4.2 shows the details of Series II poles.

4.3.4 Series III

Series III included five new poles; three Class-3 Red Pine poles, and two Class-3 Western red Cedar ones. All poles in this series were intentionally made deficient prior to undergoing the rehabilitation procedure. A 10-mm thick notch was made into each pole in this series at 914 mm (3 ft) above the ground line, perpendicular to the longitudinal axis of the pole, using a chainsaw. This cut extended to the mid-height of the cross-section, representing a 50% cross-sectional reduction at the notched zone. The rehabilitation procedure started with cleaning the notch before filling it with Pecker Patch (Crosslink Technology Inc. 2002). After the filler

material was cured, two specimens (N-3RP-6-T and N-3RP-6-C) were rehabilitated using sprayed GFRP, one with NSM GFRP bars only (N-3WC-0-TB), and another one with a combination of NSM bars and sprayed GFRP (N-3WC-6-TB), whereas one pole was tested without any further rehabilitation as a benchmark (N-3RP-0-T). For all the poles tested in this series, the poles were prepared in the test setup so that the notched region is at the tension zone of the cross-section during loading, except for N-3RP-6-C which was configured in the test setup to have the notched region at the compression zone of the cross-section. The details of Series III poles are shown in Figure 4.3.

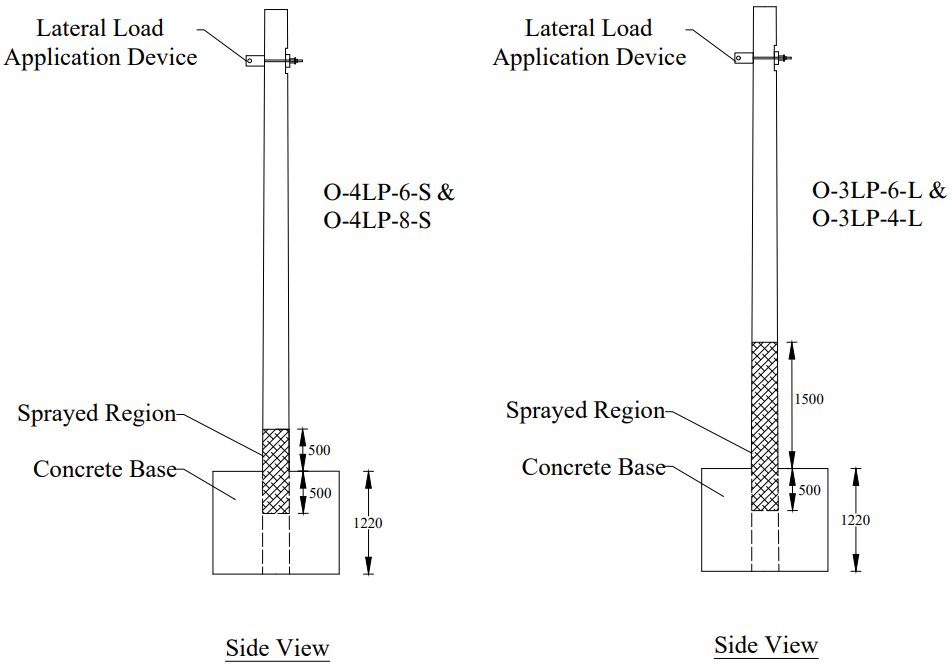

Figure 4.2 : Schematic of Series II poles, (a) Specimens O-4LP-6-S and O-4LP-8-S, and (b) Specimens O-3LP-4-L and O-3LP-6-L (Dimensions in mm)

Furthermore, the specimens sprayed with GFRP had a layer thickness of 6 mm that extended 650 mm above and below the notched zone. The length of the sprayed zone was specifically chosen to completely cover the NSM GFRP bars for specimen N-3WC-6-TB, while enabling

meaningful comparison against the other specimens in this series (i.e., by avoiding any possible effect of different lengths of sprayed GFRP layers).

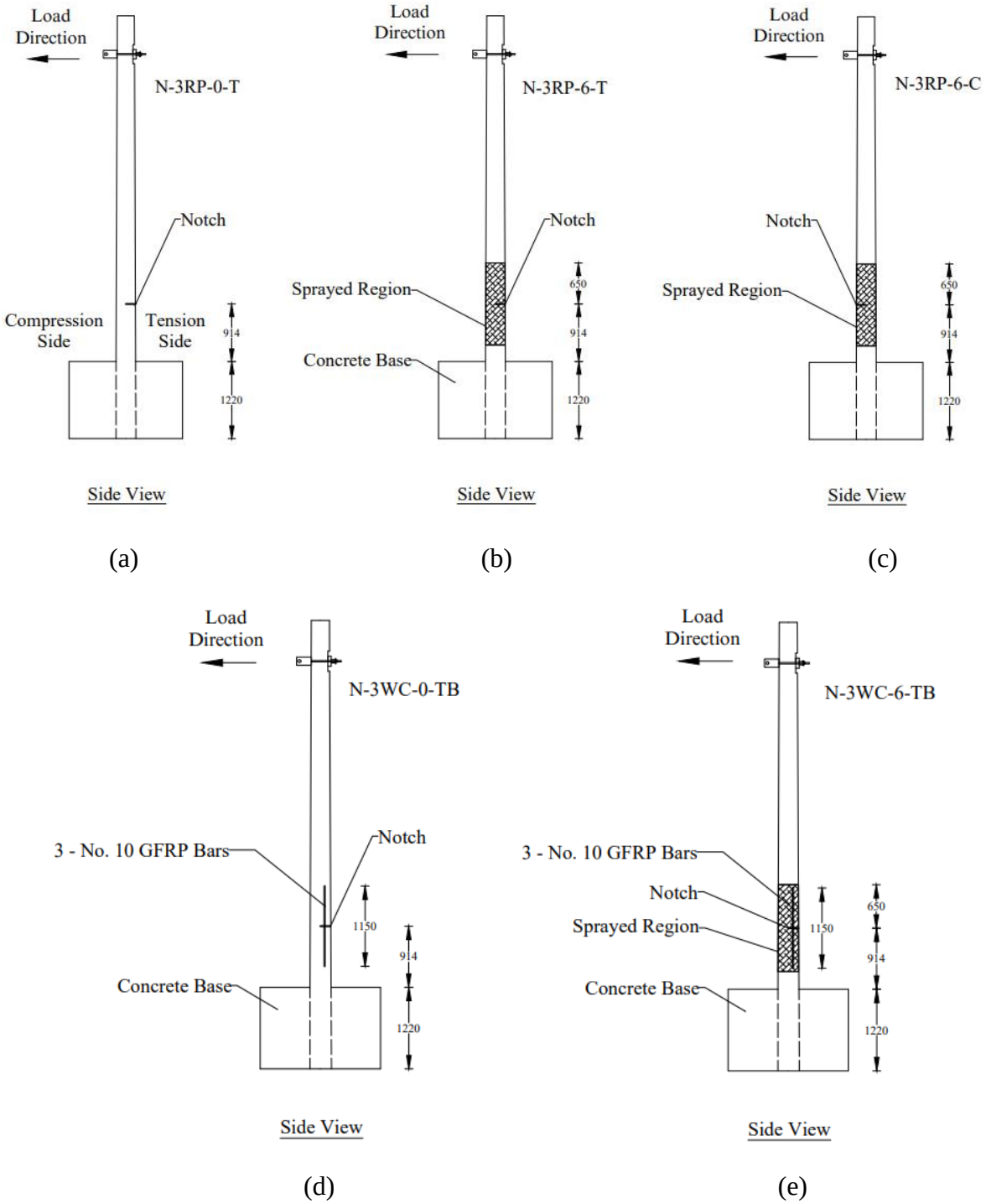

Figure 4.3: Schematic of Series III poles, (a) Specimen N-3RP-0-T, (b) Specimen N-3RP-6-T, (c) Specimen N-3RP-6-C, (d) Specimen N-3WC-0-TB, and (e) Specimen N-3WC-6-TB (Dimensions in mm)

Moreover, the location of the notched zone and the associated length of the sprayed zone were outlined to have the rehabilitated region away from the ground line to evaluate the efficiency of the rehabilitation technique shifting away the failure from the deficient notched zone.

For the specimens that incorporated NSM-GFRP bars as a part of their rehabilitation technique, three 15-mm (0.6-in.) wide × 20-mm (0.8-in.) deep × 1200-mm (4-ft) long grooves were made into the poles on the tension zone. The grooves were symmetric about the notch in the longitudinal direction and evenly distributed along the half-perimeter of the tension zone as shown in Figure 4.4 (a) and (c). Then a 1.15-m long, No. 10 (9.5-mm diameter) GFRP bar was glued into each groove using the Rotafix Structural Adhesive (Rotafix Northern Ltd. 2023) along with the associated powder additive, as mentioned earlier. Figure 4.4 (b) shows the layout of the NSM GFRP bars on the tension side of the wood pole.

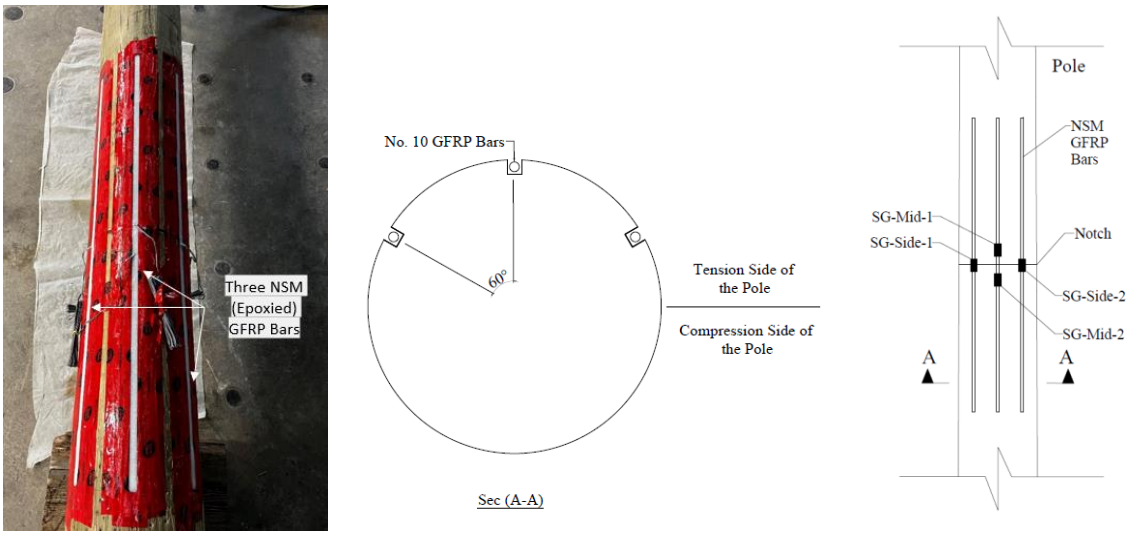

(a) (b) (c)

Figure 4.4: Details of NSM-GFRP bars layout

4.3.5 Rehabilitation process

For all the sprayed poles in this study, the spray process was the same. A booth, with a unique ventilating system designed for the laboratory, was built and placed near the laboratory door,

covered by plastic sheets. During the spraying process, the poles were hung vertically using a crane, while the prospective sprayed region of the pole was placed in the special booth where the spraying is performed. The bottom of the pole was controlled using a demountable rotating steel rod. For each retrofitted pole, a thin layer of resin was sprayed first to enhance the bonding performance between the sprayed-GFRP composites and the wood. After that, the GFRP composites were sprayed while rotating the pole. Small hand rollers were used to achieve a uniform thickness over the sprayed region and force the entrapped air out. Rolling also helped fill the small holes and cracks on the pole surface with the composite. Further spraying and rolling were repeated until the desired thickness was achieved, which was checked against foam pieces cut to the required thickness of the composite and attached above and below the sprayed region of each pole as shown in Figure 4.5.

(a) (b) (c) (d)

Figure 4.5: Spraying process: (a) Pole setup, (b) GFRP spraying, (c) Rolling the sprayed composite, and (d) Sprayed composite left to cure

4.4 Test Setup and Procedure

Considering most of the loads acting on the utility poles in service are in the horizontal direction,

all pole specimens were tested in a vertical position according to the requirements of ASTM D1036–99 (ASTM D1036–99 2017) using the cantilever test method. This was achieved by connecting the loading point of the pole to a crane using a steel cable. A hole was drilled at 610 mm (2.0 ft) from the upper end of each pole and a notch was made around that hole on the tension side of the pole to install the lateral load applying system. The lateral load was applied to the pole using a steel cable, connected to the pole at the loading point from one end and to a 10-tonne capacity overhead crane (moving upward at a constant speed during test) on its other end and passing through a set of pulleys in between. Figure 4.6 shows the side view of the top part of the test setup during a test, and Figure 4.7 shows the test setup schematic.

Figure 4.6: Side view of the test setup (top part) during a test

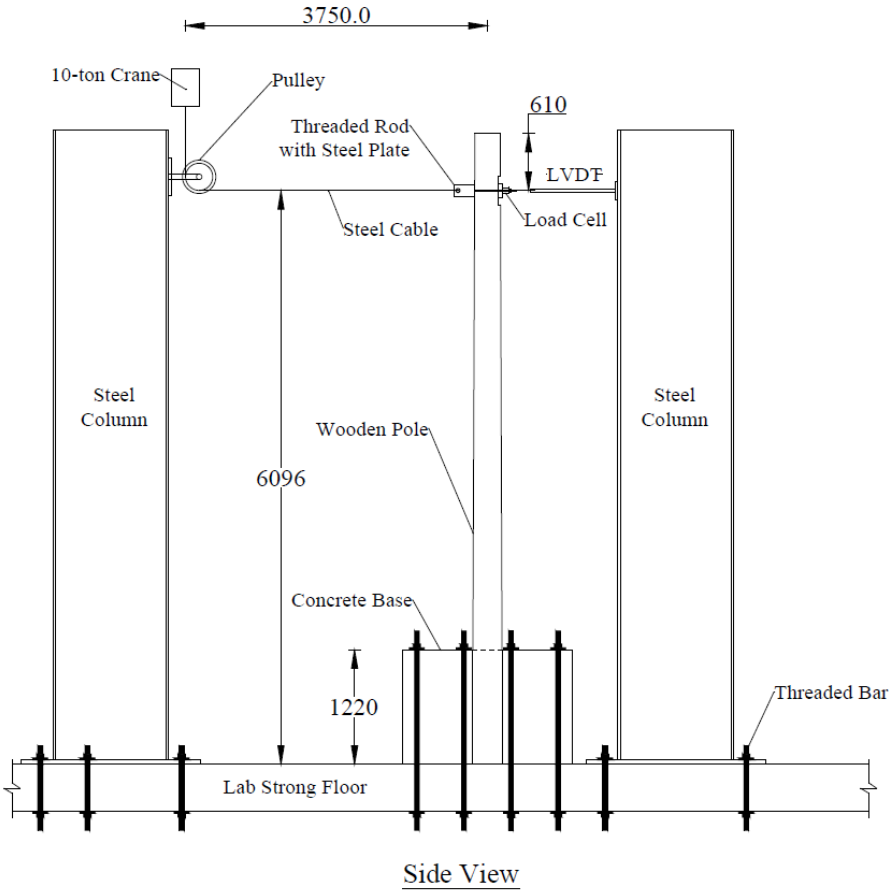

(a)

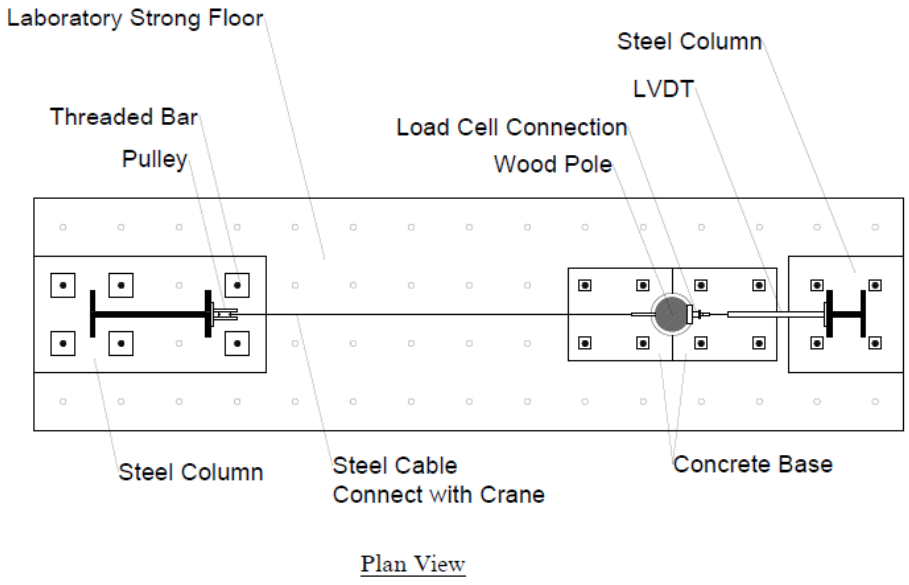

(b)

Figure 4.7: Schematic drawing of the test setup, (a) Side view, and (b) Plan view

To simulate the pole embedment below the ground line, a 1.22-m (4.0-ft) high reinforced

concrete (RC) base was used. This RC base comprised of two identical concrete blocks, and each block was cast separately and reinforced with 20M GFRP bars. Each concrete block was 800 × 900 × 1,220 mm with a semi-cylindrical void on one side, forming a cylindrical void (with a slightly larger diameter than that of the poles) when the two blocks are brought together (Figure 4.8). The void had a 365-mm diameter since a 355 mm (14 in.) Sonotube with a 5 mm wall thickness was used to form the semicylindrical shape during the concrete cast. Concrete was poured into Sonotube before the blocks, to avoid any deformation caused by the concrete pressure while casting the blocks. To provide proper fixity for the RC base, both blocks were tied down to the laboratory strong floor using eight all-threaded high-strength steel bars. Then the pole specimen was placed vertically inside the cylindrical void of the RC base.

Figure 4.8: Concrete base in the laboratory

The clearance between the pole and the concrete base was filled with a thin layer of non-shrink grout up to mid-height of the RC block (bottom 2 ft). The grout at the bottom section can steadily hold the pole during the test even if the poles were not in regular shape and were naturally bent in different directions. In addition, the grout was used to compensate for the

difference in the embedment length below the ground line between the lab (4.0 ft) and the field (6.0 ft). The remaining gap (top 2 ft) was filled with fine sand. The reason for using sand rather than using grout is that it can better simulate reality and avoid having excessively rigid connection for the pole near the ground line. It also prevents the sprayed-GFRP composites from touching the grout which may result in other unexpected failure modes. Since the small amount of leaking grout filled the interspace between concrete blocks, it is hard to separate two concrete blocks after testing if leaking happens and it is also difficult to clean up when switching pole specimens. To deal with this problem, a thin layer of Dural Fast Set Epoxy Gel was used to cover the hollow section and the contact areas between the two blocks, in addition, backer rods were used to seal the bottom of both concrete blocks and vertically along the concrete block to prevent the grout leaking. A small amount of grout near the pole at 2.0-ft high was removed to form convex rounded edges after hardening so that the pole specimens will not be damaged by the grout during the test. Since every pole specimen has different dimensions and not all of them are perfectly cylindrical, the use of this new concrete base setup can lower the possibility of pole twisting or moving during the test. Figure 4.9 shows details of fillers between the pole and the base.

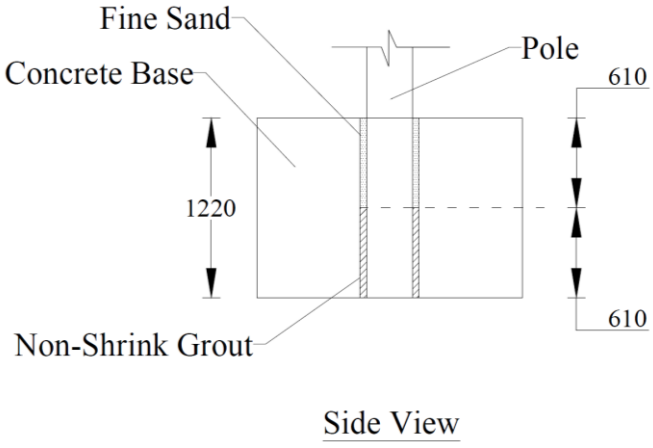

Figure 4.9: Details of fillers between the pole and base (Dimensions in mm)

4.5 Instrumentation

A compressive load cell was used to measure the real-time load during the test. As mentioned in the test setup section, pole specimens were notched at the load point (610 mm from the top), to create a flat surface to install the load cell and the setup to connect steel cable. The capacity of the used load cell is 50 tons (100,000 lbs).

To obtain the deflection of the wood poles at the loading point, a linear variable displacement transducer (LVDT) was installed at the height of 6.10 m (20.0 ft) above the laboratory strong floor. In addition, to measure the strains in the NSM-GFRP bars, four electrical strain gauges were installed near the mid-length on the outer surface of each bar as outlined in Figure 4.5 (b). All the aforementioned instrumentation was connected to a computerized Data Acquisition System to collect the measurement data, as shown in Figure 4.10.

Figure 4.10: Data Acquisition System

4.6 Test Results and Discussion

4.6.1 Adjusted code requirements for horizontal load capacity

The horizontal load requirements for the different pole classes and species are provided in CSA O15-15 (CSA 2019), which are based on the calculations for the wood tensile strength at the outermost tension fibre at the groundline section. However, such load capacities cannot be

directly compared against the experimental results of this study since all the tested poles were cut to accommodate lab height and equipment limitations (Figure 4.1). Therefore, the load requirements were adjusted to obtain the same tensile strength at the groundline section. The modified horizontal load requirements ($F_{modified}$) are calculated using the Equation below:

$$F_{modified} = F_{original}\left(\frac{L_{original}-1{,}829-610}{L_{cut}-h-610}\right) \quad \text{Equation 4.1}$$

where $F_{original}$ is the original horizontal load requirement from the CSA O15-15 (CSA 2019). $L_{original}$ is the original length of the wood pole (12,192 mm [40.0 ft] for this study), and L_{cut} is defined as the length of the cut pole specimen (i.e., 6,706 mm [22.0 ft]). The length 1,829 mm (6.0 ft) refers to the embedment length of the pole into the ground in practice, whereas *h* is the height of the concrete base at the laboratory (i.e., 1,220 mm [4.0 ft]). The length 610 mm (2.0 ft) refers to the distance between the loading point and the top of the pole. Table 4.3 shows the original and modified horizontal load requirements. A correction factor of 0.95 was applied for RP and WC poles in Table 4.3 as required by CSA O15-15 (CSA 2019).

Table 4.3: Horizontal Load Requirements

Pole class and species	Type	CSA horizontal load requirement [a] (kN)	Modified CSA load requirement [b] (kN)	Experimental ultimate load [d] (kN)
3 RP	New	12.6	25.3	37.6
3 WC	New	12.6	25.3	28.0
3 DF & LP	New	13.3	26.6	-
	Old	-	-	23.9
4 LP	New	10.7	21.4	-
	Old	-	-	19.2[c]

[a] Determined as per Table B.1 of CSA O15-15 (CSA 2019).
[b] Calculated as per Eq. (4.1).
[c] Calculated based on the experimental load for Class 3 DF and the ratio between Class 3 and 4 as per Table B.1 of CSA O15-15 (CSA 2019).
[d] Experimental ultimate loads for control specimens.

4.6.2 Series I – Control Specimens

Three Class-3 poles (O-3DF-0-X, N-3RP-0-X, and N-3WC-0-X) were tested to serve as the control specimens. Since the horizontal load requirements of CSA-O15-15 (CSA 2019) are the same for DF and LP poles, the pole O-3DF-0-X was used as a control specimen for the Class-3 LP retrofitted old poles (i.e., O-3LP-4-L and O-3LP-6-L). Nonetheless, an estimated ultimate horizontal load value was developed as a control value for the Class-4 LP retrofitted old poles (i.e., O-4LP-6-S and O-4LP-8-S) by dividing the ultimate horizontal load value of O-3DF-0-X by the ratio between the horizontal load requirements of Classes 3 and 4 LP poles according to CSA-O15-15 (CSA 2019). Table 4.3 shows the test results for control specimens and the estimated ultimate loads. The poles N-3RP-0-X and N-3WC-0-X were used as control specimens for the notched and rehabilitated poles of series III, as appropriate.

The load-deflection response of wooden poles is somewhat complex since wood is a non-homogenous and anisotropic material. As shown in Figure 4.11, specimen N-3RP-0-X behaved mostly linear up to about 72% of its horizontal load resistance, followed by a minor softening in its response until the pole failed at 37.6 kN. The load-deflection response of N-3WC-0-X exhibited softening beyond approximately 64% of its horizontal load resistance, followed by few sudden drops in load resistance. Yet the response exhibited strength gain after each drop until the pole failed at 28.0 kN. The old control pole specimen O-3DF-0-X exhibited early degradation of strength at about 3.0 kN horizontal load resistance, followed by a linear response, with few minor drops in load resistance, up to about 75% of its horizontal load resistance. Then softer response was exhibited until the pole failed at a horizontal load of 23.9 kN. The poles N-3RP-0-X and N-3WC-0-X exceeded the horizontal load requirement of CSA O15-15 (CSA

2019), whereas O-3DF-0-X did not achieve its respective horizontal load requirement. This agrees well with the description of each pole since the first two were at their at-installation state whereas the latter was denoted as an old, dismissed pole.

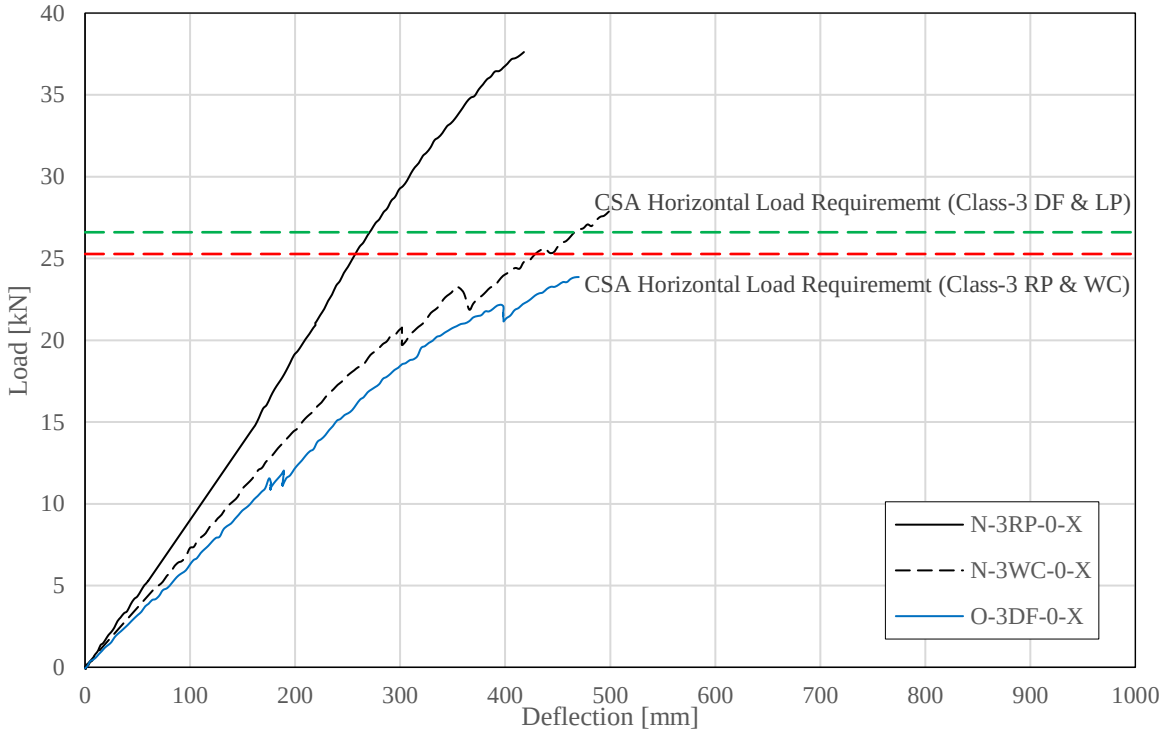

Figure 4.11: Load-deflection relationship at loading point – Series I: control poles

All control poles failed by rupture on the tension side between 500 to 1000 mm above the ground line. For the control old pole O-3DF-0-X, the failure occurred progressively (section by section) and gradually. An example of failure mode is shown in Fig. 4.12.

4.6.3 Load-carrying capacities and failure modes – Series II poles

Table 4.4 shows the ultimate loads and corresponding deflections for Series II poles. The sprayed-GFRP layer prominently increased the load-carrying capacity of the retrofitted old poles (i.e., O-4LP-6-S, O-4LP-8-S, O-3LP-4-L, and O-3LP-6-L) to exceed the requirements of CSA O15-15 (CSA 2019), as shown in Figs. 4.13 and 4.14. The 1.0-m long sprayed-GFRP layer increased the old poles (O-4LP-8-S and O-4LP-6-S) load-carrying capacity by 28% and

38%, respectively, compared to the estimated capacity of the Class-4 LP control old pole (19.2 kN).

Table 4.4: Test results for Series II poles

Specimen ID	Ultimate load (kN)	Loading point deflection at failure load (mm)
O-4LP-6-S	26.5	425
O-4LP-8-S	24.5	499
O-3LP-4-L	45.9	427
O-3LP-6-L	34.1	558

Figure 4.12: Typical failure mode for control poles (pole N-3WC-0-X)

In addition, the sprayed-GFRP retrofitting restored the old pole load-carrying capacity up to 114% and 124% of its at-installation capacity as per CSA O15-15 (21.4 kN) for O-4LP-8-S and O-4LP-6-S, respectively. However, with this 1.0-m (3.3-ft) long sprayed-GFRP layer, the ultimate load-carrying capacity did not increase as the thickness of the GFRP layer increased from 6 to 8 mm in specimen. On the other hand, the 2.0-m (6.6-ft) long sprayed-GFRP layer

increased the horizontal load capacity of O-3LP-4-L and O-3LP-6-L by 92% and 43%, respectively, compared to the capacity of the control old pole O-3DF-0-X (23.9 kN). Furthermore, retrofitting with sprayed GFRP did not only restore the load-carrying capacity of the poles to meet the CSA O15-15 requirement (26.6 kN), but it also exceeded that capacity requirement by 73% and 28% for poles O-3LP-4-L and O-3LP-6-L, respectively.

All poles failed suddenly on the tension side, where the failure occurred above the sprayed-GFRP layer for the retrofitted poles in this series as shown in Figure 4.15 (a). No failure was observed for the GFRP layer for the retrofitted poles except for O-3LP-4-L, which experienced tensile rupture along with delamination of the sprayed layer (Figure 4.15 [b]) at a much higher ultimate load compared to the other poles. This may indicate that the limited thickness of 4 mm for the sprayed GFRP layer was more compatible with the wooden pole than the larger thicknesses, resulting in an effective composite action that led to a much higher load carrying capacity for the retrofitted pole. On the other hand, the 6- and 8-mm thicknesses imposed significant confinement on the retrofitted poles, forcing the failure to occur away from the sprayed zone. The fact that the failure occurred right above the sprayed zone for poles O-4LP-6-S, O-4LP-8-S, and O-3LP-6-L may also indicate stress concentration at the transition from the retrofitted zone to the exposed portion above. It may be recommended to use 6-mm thick sprayed GFRP layers or larger to retrofit old poles with an adequate length such that the lever arm of the exposed portion required an equivalent horizontal load to cause failure to that causing rupture of the GFRP layer at the ground line.

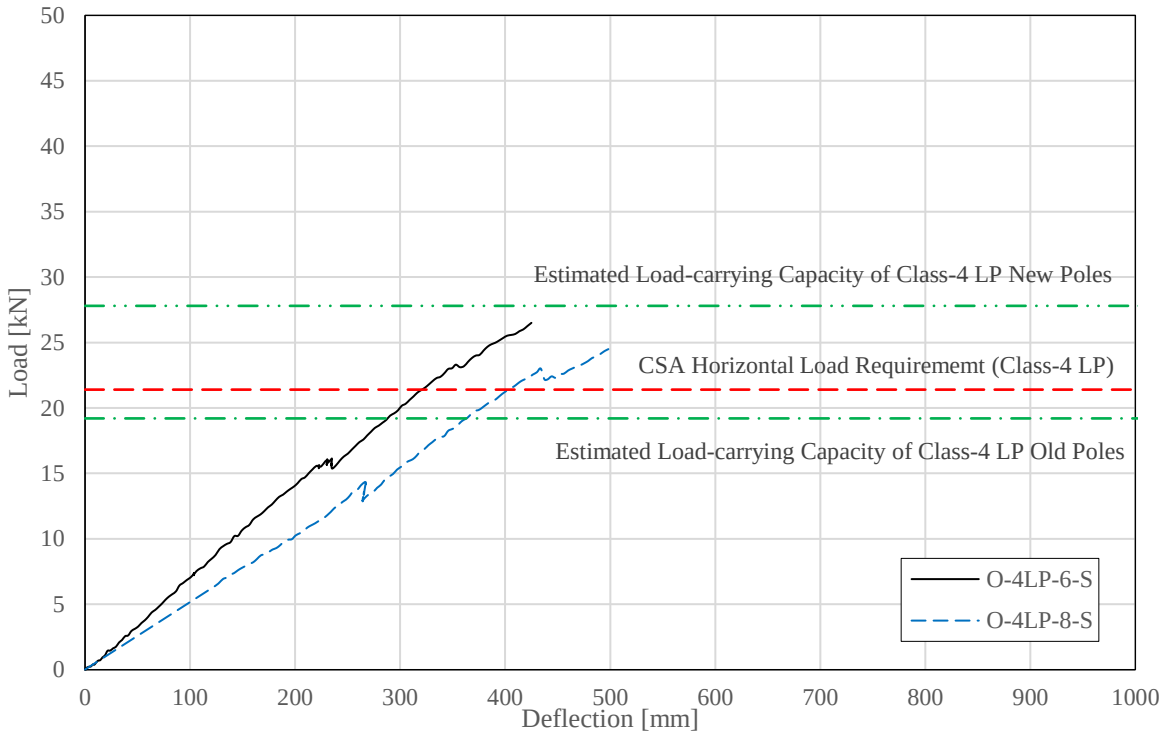

Figure 4.13: Load-deflection relationship at loading point – Class-4 Series II poles

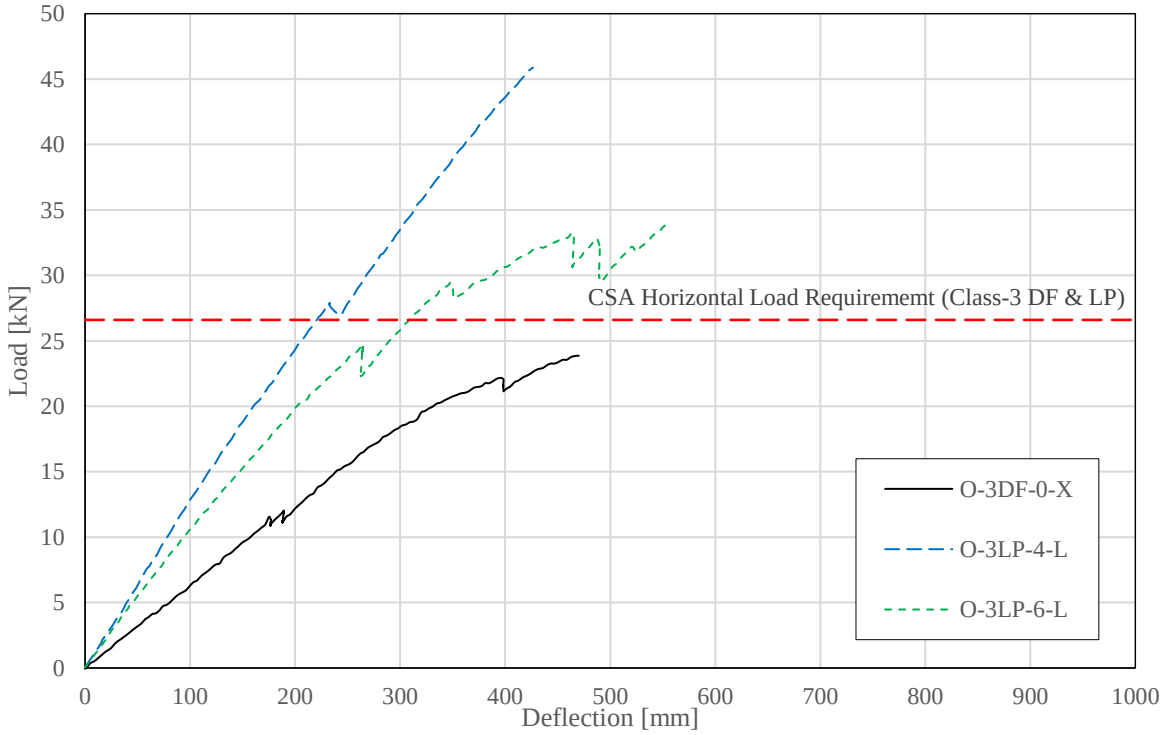

Figure 4.14: Load-deflection relationship at loading point – Class-3 Series II and control pole

(a) (b)

Figure 4.15: Failure modes – Series II poles, (a) Specimen O-4LP-6-S, and (b) Specimen O-3LP-4-L

4.6.4 Load-deflection relationship – Series II poles

Figures 4.13 and 4.14 show the load-deflection relationships at the loading point for series II poles. Since no control new poles with the same classes and species as those of series II poles were tested, the discussion is limited to the stiffnesses of the tested old poles only (since there is no specific code requirement for the stiffness of the utility poles). As shown in Fig. 4.13, the stiffness of the specimen O-4LP-8-S was lower than that of specimen O-4LP-6-S, while both specimen O-4LP-8-S and O-4LP-6-S have the same class and species and O-4LP-8-S had larger sprayed-GFRP layer thickness, such difference in stiffness may have occurred due to the individual differences between the poles. Similar observations were reported by Kell (2001). The aforementioned differences can also be more acceptable considering the fact that each pole was probably decommissioned after a different number of service years and/or exposure to

different conditions. Figure 4.14 shows the load-deflection relationship at the loading point for specimens O-3DF-0-X, O-3LP-4-L, and O-3LP-6-L. The sprayed poles O-3LP-4-L and O-3LP-6-L had higher stiffness than the old control pole O-3DF-0-X. Moreover, specimen O-3LP-4-L exhibited a higher stiffness than O-3LP-6-L since the reinforcing effect of the GFRP layer were fully utilized, as corroborated by the fact that the pole failed by combined rupture of the wood and the retrofitting layer.

4.6.5 Load-carrying capacities and failure modes – Series III poles

Since the targeted outcome of the rehabilitation of series III poles was to shift the failure away from the notched area, failure of the sprayed-GFRP layer was not acceptable. Therefore, based on the test observations of series II poles, it was decided to utilize the 6-mm thick sprayed-GFRP layer for series III poles. Table 4.5 shows the ultimate loads for Series III. The ultimate load capacity of the notched reference pole (N-3RP-0-T) and the pole that was rehabilitated by NSM GFRP bars only (N-3WC-0-TB) are much lower than the requirements (25.3 kN) of CSA O15-15 (CSA 2019). The 50-% cross-sectional area reduction decreased the load-carrying capacity of the reference pole (N-3RP-0-T) by approximately 79% compared to the ultimate load of the control pole (N-3RP-0-X).

Table 4.5: Test results for Series III poles

Specimen ID	Ultimate load (kN)	Loading point deflection at failure Load (mm)
N-3RP-0-T	8.0	145
N-3RP-6-T	27.1	554
N-3RP-6-C	34.1	414
N-3WC-0-TB	11.0	760
N-3WC-6-TB	26.3	465

It can obviously be inferred from Table 4.5 that rehabilitating the poles using NSM GFRP bars only (i.e., pole N-3WC-0-TB) was inefficient, since it hardly achieved a horizontal load capacity equal to 39% of that of the control pole N-3WC-0-X. The sole effect of the NSM GFRP bars on the ultimate load capacity is rather insignificant compared to that of the sprayed-GFRP, as will be discussed later. Increasing the amount and size of the GFRP bars might achieve a better outcome. However, based on the current results from this study and considering the time and resources used to apply the NSM GFRP bars, it can be concluded that using NSM GFRP bars, with the size, length and application method used in this study, to rehabilitate wooden utility poles is not a structurally efficient or cost-effective option compared to using sprayed FRP, as will be discussed below.

All sprayed poles, N-3RP-6-T, N-3RP-6-C, and N-3WC-6-TB, achieved or exceeded the load-carrying capacity requirements of CSA O15-15 (CSA 2019), as shown in Figures 4.16 and 4.17. With the notch on the tension side of the pole (N-3RP-6-T), the sprayed-GFRP layer was able to restore about 72% of its at-installation load-carrying capacity (i.e., load capacity of pole N-3RP-0-X of 37.6 kN). The restored load capacity increased to 91% when the notch was on the compression side of the pole (i.e., N-3RP-6-C).

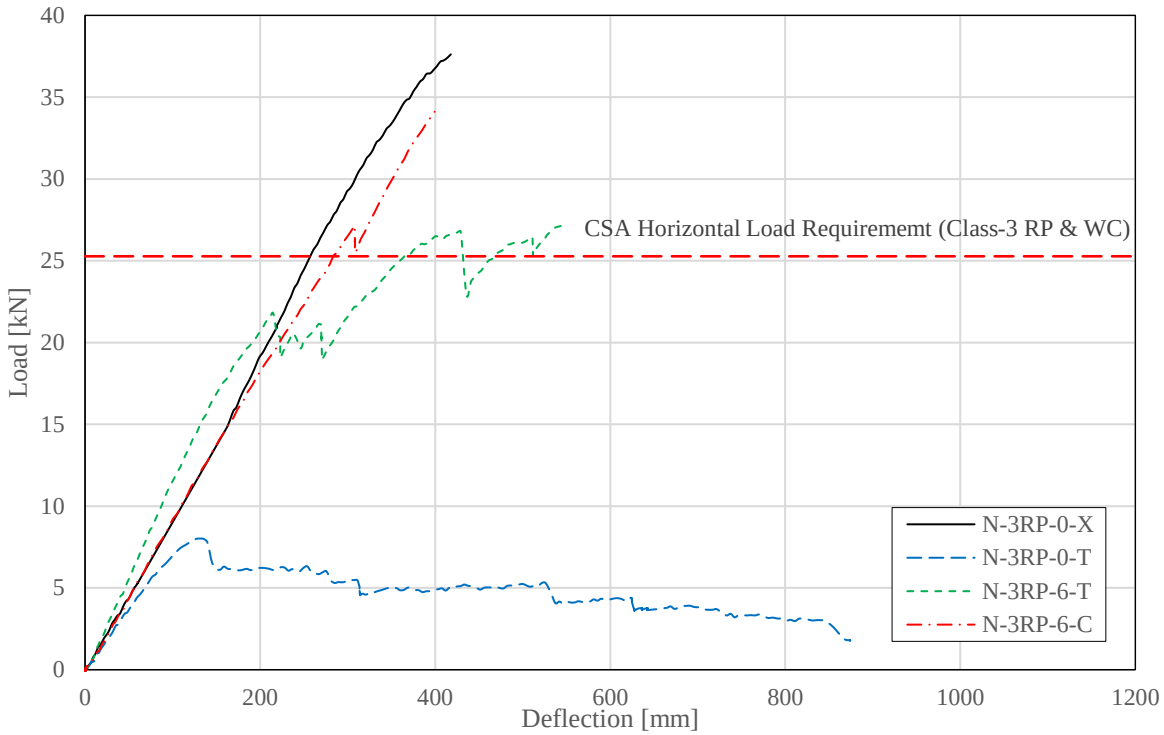

Figure 4.16: Load-deflection relationship at loading point – Class-3 RP Series III and control pole

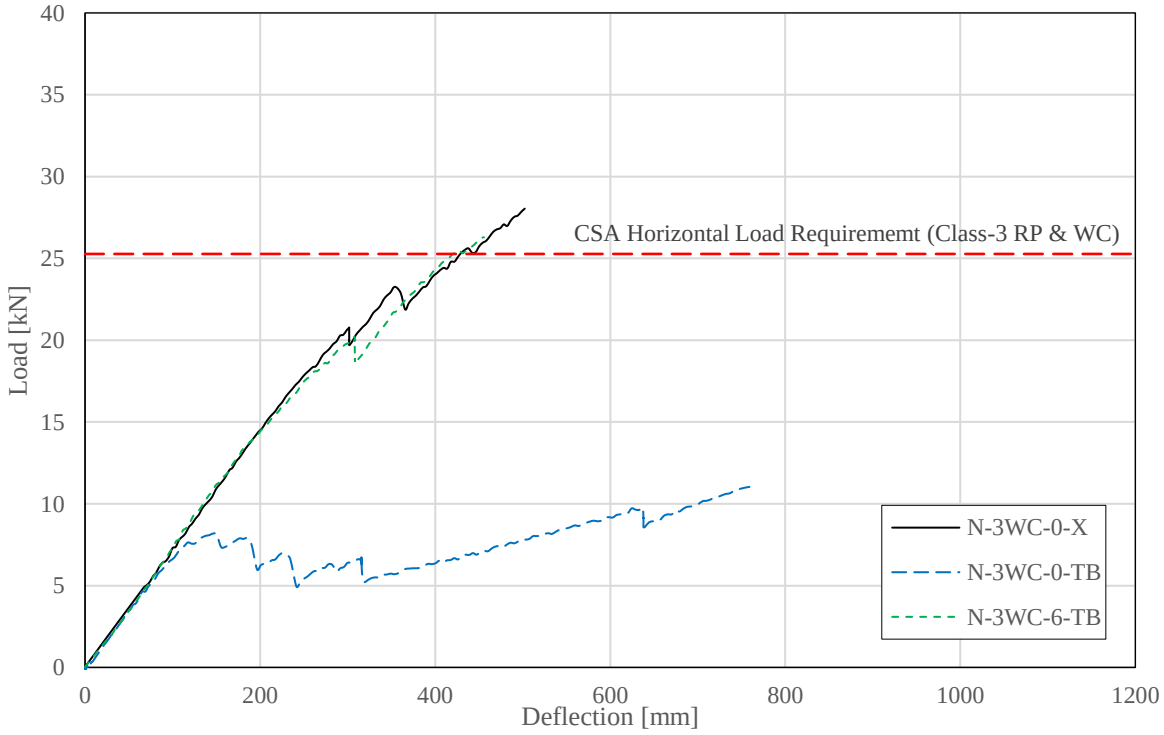

Figure 4.17: Load-deflection relationship at loading point – Class-3 WC Series III and control pole

Installing NSM GFRP bars at the notched zone on the tension side of the pole prior to spraying the GFRP layer provided the pole N-3WC-6-TB with 94% of the at-installation load-carrying capacity of the control pole N-3WC-0-X. This represents an increase of 31% compared to the restored load capacity when only GFRP spraying was used to repair the notched pole N-3RP-6-T, which indicates more efficiency for the combined rehabilitation scheme of GFRP spraying along with NSM GFRP bar installation. Nonetheless, there would be a tradeoff between the anticipated gain in load-carrying capacity and the added complexity of installing the NSM bars.

Both un-sprayed poles N-3RP-0-T and N-3WC-0-TB failed at the notched section. The filler material was detached from the wood and a vertical crack initiated at the mid-height of the notched section and extended downwards to the ground line, through which (i.e., the vertical crack) each pole was split into two parts as shown in Figures 4.18 (a) and (b). For specimen N-3WC-0-TB, the NSM GFRP bars were de-bonded (or partially de-bonded) as shown in Figure 4.18 (b). For the sprayed poles (N-3RP-6-T, N-3RP-6-C, and N-3WC-6-TB), the failure occurred below the sprayed region as shown in Figures 4.18 (c) and (d), while no failure occurred at the notch when the failure started below the spray region as shown in Figure 4.18 (e). In addition, the failure occurred on the tension side for poles N-3RP-6-T, N-3RP-6-C, whereas crushing on the compression side took place for N-3WC-6-TB, with a portion of the bark delaminated on the tension side (Figure 4.18 [d]). It is worth noting that some delamination was observed for the sprayed GFRP layer near the notched section for poles N-3RP-6-T, and N-3WC-6-TB, whereas no delamination was reported for N-3RP-6-C.

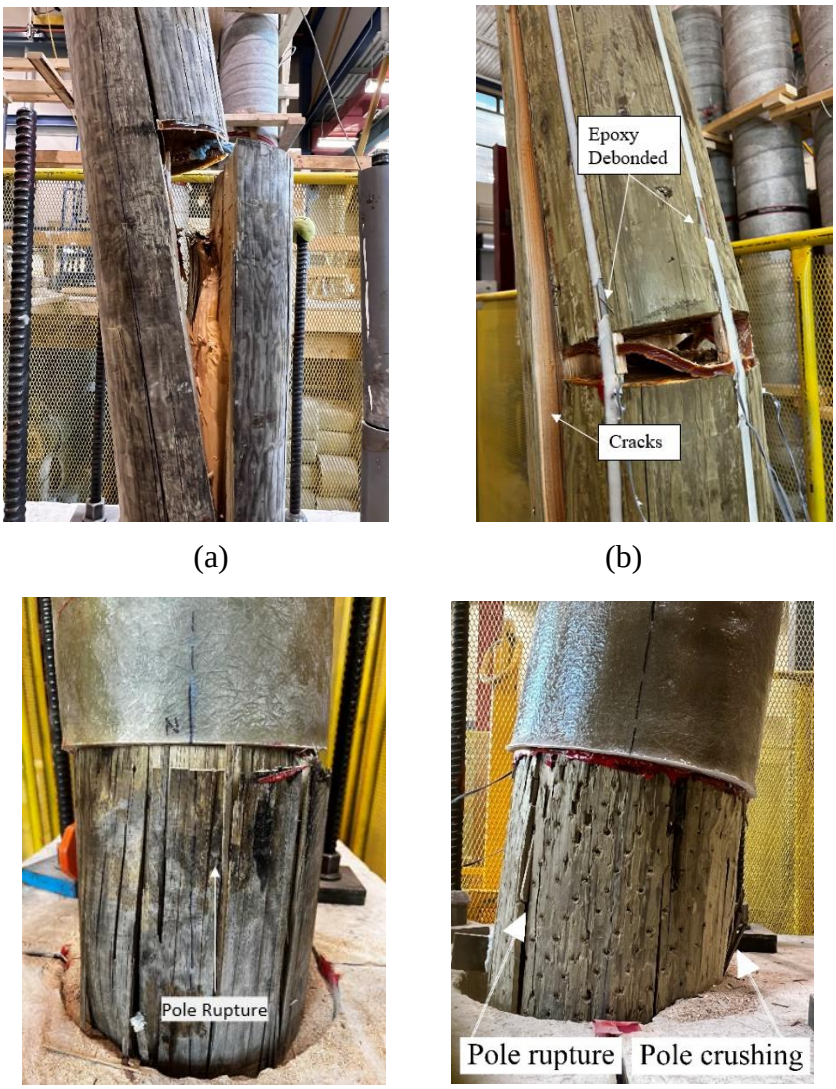

(a) (b)

(c) (d)

Figure 4.18: Failure modes – Series III poles, (a) Specimen N-3RP-0-T, (b) Specimen N-3WC-0-TB, (c) Specimen N-3RP-6-C, and (d) Specimen N-3WC-6-TB

Following the completion of the tests, a 150-mm wide strip of the sprayed GFRP layer, centered at the notched section, was cut and removed for specimen N-3RP-6-T, as shown in Figure 4.19. The wood filler de-bonded at several spots, and some wood damage was observed near the notched zone. This may indicate that some strength degradation occurred due to damage at the reduced section. However, the sprayed GFRP layer was able to effectively confine the pole, preventing further damage around the notched zone and forcing failure to occur outside the

sprayed region. In a similar manner, the whole sprayed GFRP layer was removed following the testing of N-3WC-6-TB, where cracks and spalling of the epoxy resin was noticed at several locations, indicating the debonding of the NSM bars, as shown in Figure 4.20. Nevertheless, such debonding of the NSM bars was attributed to the abrupt failure below the sprayed region at the end of the test, which may have caused instability to the rest of the pole above, including the NSM bars. This is corroborated by the load-strain relationships for the NSM bars, as discussed later.

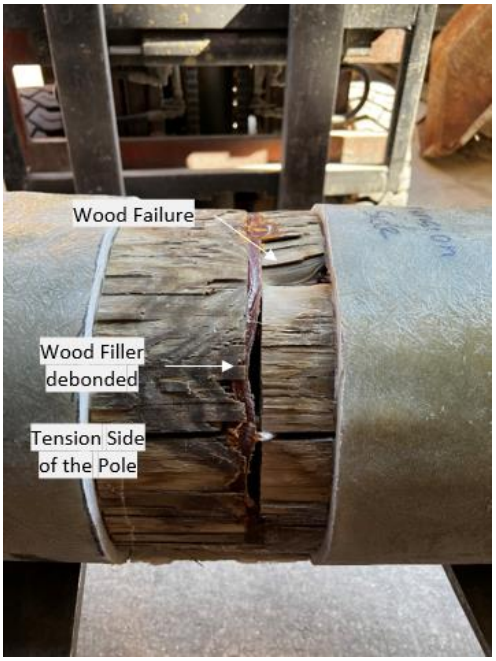

Figure 4.19: Details at groove after the test – specimen N-3RP-6-T

(a) (b)

Figure 4.20: Epoxy conditions after the test for specimen N-3WC-6-TB, (a) De-bonded epoxy, and (b) Epoxy cracks

4.6.6 Load-deflections relationships – Series III poles

Figures 4.16 and 4.17 show the load-deflection relationships at the loading point for the poles tested in this series along with the control new poles. Both specimens N-3RP-0-T and N-3WC-0-TB exhibited similar initial stiffnesses to their respective control poles up to approximately a horizontal load resistance of 8.0 kN, followed by significant consecutive drops for the load-carrying capacity in addition to sharp increase of lateral deflection, which matches well the test observations for those poles. While N-3RP-0-T suffered from continuous degradation of load-carrying capacity up to failure, the pole N-3WC-0-TB started picking up strength after the deflection at the loading point exceeded 320 mm, accompanied by few drops in the load

resistance along the way until complete failure occurred. While such gains in horizontal load resistance might be due to the reinforcing action of the NSM GFRP bars, the fact that localized debonding of the NSM bars occurred at a horizontal load of about 8 kN makes it difficult to be confirm the aforementioned reason. This is further clarified by the load-strain responses for the NSM bars, as discussed later. Generally, the overall load-deflection response of N-3WC-0-TB indicates an inadequate composite action where the NSM bars on their own were not able to prevent or suppress the deterioration that commenced at the notched section.

As shown in Figure 4.16, specimen N-3RP-6-C reached a higher ultimate load than that of N-3RP-6-T, yet both poles achieved the horizontal load requirement of CSA O15-15 (2019). The ultimate load of N-3RP-6-T and N-3RP-6-C was 72% and 91% that of the control pole N-3RP-0-X, respectively. The higher initial stiffness of N-3RP-6-T can be attributed to the individual differences between the poles. For the same pole, the fluctuating load-deflection response exhibited beyond approximately 22 kN may indicate the onset of wood damage and filler separation at the reduced section, before the sprayed GFRP layer was able to contain the pole and more strength gain was experienced. The major load drop at about 425 mm lateral deflection can be considered as the onset of failure for the rehabilitated pole, where no further gain (over the achieved load capacity) was noticed afterwards. The combination of damage at the reduced section as well as below the sprayed region might be the reason for such turbulent load-deflection response for N-3RP-6-T. On the other hand, a smooth load-deflection response was exhibited by N-3WC-6-TB (Figure 4.17), which reflects an optimum combination of NSM GFRP bars and sprayed GFRP for rehabilitation of notched poles, producing a behavior similar to that of the un-notched control pole.

4.6.7 NSM-GFRP bars strains

Figures 4.21 and 4.22 show the load-strain relationships for the strain gauges attached to the NSM GFRP bars implemented in specimens N-3WC-0-TB and N-3WC-6-TB, respectively. As expected, larger strains were developed in the bars at the outermost fibre compared to those at the bars installed on the sides. For specimen N-3WC-0-TB, stable load-strain relationships can be observed for all strain gauges up to a horizontal load resistance of 8.0 kN, beyond which the relationships started to decline, indicating the onset of debonding of the NSM bars. For specimen N-3WC-6-TB, one strain gauge on a side bar was not functioning prior to the commencement of the test, while the strain gauge on the other side bar malfunctioned at a load equal to 10.7 kN. However, the strain gauges on the central NSM bar showed a stable load-strain response with a slope that increased after the load reached 20.0 kN, which might be related to the load drop exhibited on the load-deflection response (Figure 4.18). This can also be a result of the observed delamination of the sprayed GFRP layer, which may justify the slope increase for the load-strain response of the NSM bars (i.e., larger contribution of the NSM bars as a result of partial delamination of the sprayed GFRP layer).

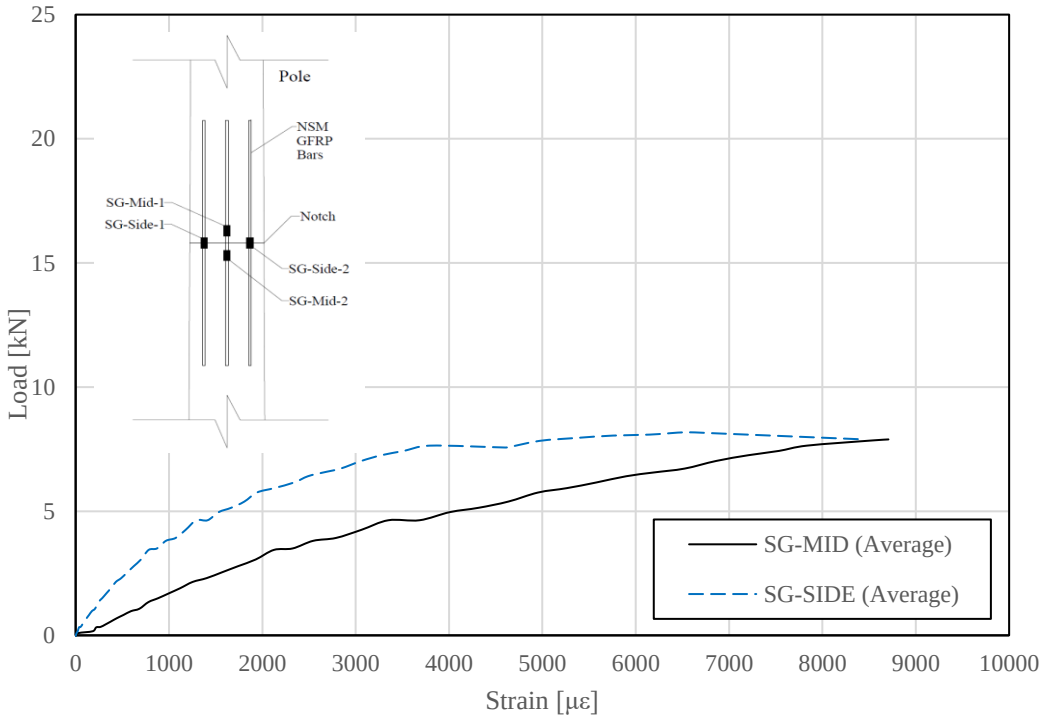

Figure 4.21: Load strain relationship for all NSM GFRP bars on specimen N-3WC-0-TB

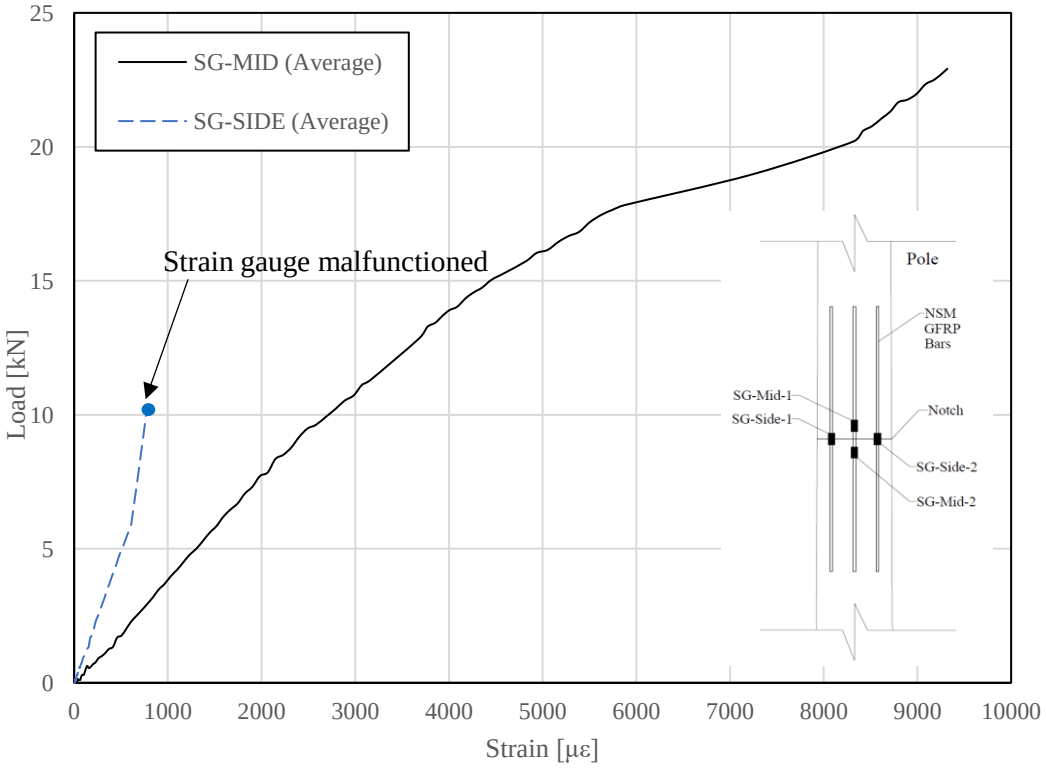

Figure 4.22: Load-strain relationship for all NSM GFRP bars on specimen N-3WC-6-TB

The load-strain relationship was maintained up to a horizontal load resistance of approximately 23 kN, where the strain gauges malfunctioned afterwards. While it was difficult to determine

visually if the NSM bars experienced any debonding at that load level (i.e., since they were hidden underneath the sprayed GFRP), the stable load-deflection response exhibited by the pole up to failure confirms that no premature debonding occurred to the NSM GFRP bars. In addition, Comparing the load-strain graphs of specimens N-3WC-0-TB and N-3WC-6-TB It can also be noticed that at the same load level, the strains developed in the NSM bars of N-3WC-6-TB are much less than those developed in their counterparts of N-3WC-0-TB, which can be a result of the contribution of the sprayed GFRP layer by hoop and/or longitudinal tensile stresses experienced therein. Overall, this also verifies the efficiency of the composite action provided by the combination of the sprayed GFRP layer and NSM GFRP bars.

CHAPTER 5 – ANALYTICAL MODEL FOR LOAD CAPACITY AND FAILURE MODE PREDICTION

5.1 Horizontal Load Capacity Prediction

5.1.1 Contribution of Poles

Prior to testing the poles, load-carrying capacity predictions were made for the poles to be retrofitted to establish a simple analytical procedure to estimate the strength of the sprayed poles and assess the effectiveness of the retrofitting process. The following equation was used to estimate the lateral load capacity as per ASTM D1039-99 (ASTM D1036–99 2017):

$$F = \frac{32\pi^2 P(L-\Delta_L)}{C^3} \qquad \text{Equation 5.1}$$

where F is the maximum fiber stress at ground line or failure section, taken as modulus of rupture (MOR) by CSA O15-15 (CSA 2019); P is the lateral load capacity of the pole; L is the lever arm of the lateral load (i.e., distance between ground line [or failure section] and point of load application); is the longitudinal deflection of the load point at the maximum load, taken as zero herein for conservative estimation; and C is the circumference of the pole at ground line (or failure section). The values of MOR, C and P are summarized in Tables 5.1 and 5.2 for poles of series II and III, respectively. The lateral load capacity was denoted as P_o for the new pole, whereas the load capacity at the notched section (where circumference was measured as C_N) was calculated as P_N. It should be noted that P_N was calculated using the basic formula for normal stresses, considering the moment of inertia and location of the centroid according to the shape and location of the reduced section. For instance, for a 50% section reduction, the load capacity was estimated using Eq. (5.2) or (5.3), depending on whether the notch is located

on the tension or compression side, respectively.

$$F = \frac{\left(1-\frac{4}{3\pi}\right)P_N(L_N-\Delta_L)}{R_N{}^3\left(\frac{\pi}{8}-\frac{8}{9\pi}\right)} \quad \text{Equation 5.2}$$

$$F = \frac{P_N\left(\frac{4}{3\pi}\right)(L_N-\Delta_L)}{R_N{}^3\left(\frac{\pi}{8}-\frac{8}{9\pi}\right)} \quad \text{Equation 5.3}$$

where R_N is the radius of the pole at the notched section and L_N is the distance between the notched section and point of load application.

5.1.2 Contribution of GFRP Composite

The lateral load capacity of the sprayed GFRP layer, P_{FRP}, was estimated from the equation of normal stress, considering the FRP layer in tension zone only as half a circular ring having a thickness t_{FRP}.

$$f = \frac{M}{I}.y \quad \text{Equation 5.4}$$

$$M = P_{FRP}\,(L-\Delta_L) = \frac{I_{FRP}\cdot\phi_{FRP}f_{u,FRP}}{R+\frac{t_{FRP}}{2}} = \pi.t_{FRP}\left(R+\frac{t_{FRP}}{2}\right)^2\cdot\phi_{FRP}\,f_{u,FRP} \quad \text{Equation 5.5}$$

where ϕ_{FRP} is the material resistance factor of the sprayed FRP, assumed herein as unity; $f_{u,FRP}$ is the ultimate tensile strength of the sprayed FRP coupons, as listed in Table 3.3; and R is the radius of the pole at the ground line section. It is worth mentioning that for notched poles, R_N and L_N are used in Equation 5.5, and the resulting load capacity is identified as $P_{N,FRP}$.

Table 5.1: Predicted and proposed load capacities for Series II poles

Specimen ID	C (mm)	$MOR = F$ (MPa)	t_{FRP} (mm)	P_o[a] (kN)	P_{FRP}[b] (kN)	$P_{est,1}$[c] (kN)	$P_{est,2}$[d] (kN)	P_{exp} (kN)	P_{est}/P_{exp}	$P_{pro,1}$[e] (kN)	$P_{pro,2}$[f] (kN)	P_{pro}/P_{exp}
O-4LP-6-S	980	45	6	27.5	12.1	25.9	17.3	26.5	0.65	30.5	23.2	0.87
O-4LP-8-S	968	45	8	26.5	16.0	29.2	16.7	24.5	0.68	33.7	22.3	0.91
O-3LP-4-L	1,020	45	4	31.0	8.6	24.1	19.5	45.9	0.53	29.4	26.1	0.64
O-3LP-6-L	1,045	45	6	33.3	13.8	30.4	21.0	34.1	0.61	36.1	28.1	0.82

[a] Lateral load causing failure at the groundline section, estimated as per Equation 5.1 assuming a new pole.

[b] Lateral load contribution of the sprayed GFRP layer at groundline section, estimated as per Equation 5.5 using coupon tensile strength.

[c] Total lateral load capacity of the wood section and the sprayed layer, assuming the old pole capacity as one-half that of the new pole.

[d] Lateral load causing failure above the sprayed region, estimated as per Equation 5.1, assuming the old pole capacity as one-half that of the new pole.

[e] Total lateral load capacity of the wood section and the sprayed layer, assuming the old pole capacity as two-thirds that of the new pole.

[f] Lateral load causing failure above the sprayed region, estimated as per Equation 5.1, assuming the old pole capacity as two-thirds that of the new pole.

Table 5.2: Predicted load capacities for Series III poles

Specimen ID	C (mm)	C_N (mm)	$MOR = F$ (MPa)	t_{FRP} (mm)	$P_o = P_{est,1}$[c] (kN)	$P_{N,FRP}$[d] (kN)	P_N[e] (kN)	$P_{est,2}$[f] (kN)	P_{exp} (kN)	P_{est}/ P_{exp}
N-3RP-0-T[a]	1,025	995	41	_	28.7	_	7.8	7.8	8.0	0.98
N-3RP-6-T[a]	1,030	998	41	6	29.1	15.6	7.9	23.4	27.1	0.86
N-3RP-6-C[b]	992	965	41	6	26.0	14.5	9.7	24.1	34.1	0.71
N-3WC-0-TB[a]	1,070	1,027	38	_	30.2	_	8.0	8.0	11.0	0.72
N-3WC-6-TB[a]	1,065	1,032	38	6	29.8	16.5	8.1	24.6	26.3	0.94

[a] Notched on the tension side.

[b] Notched on the compression side.

[c] Lateral load causing failure at the groundline section, estimated as per Equation 5.1.

[d] Lateral load contribution of the sprayed GFRP layer at the notched section, estimated as per Equation 5.5 using coupon tensile strength.

[e] Lateral load capacity of wood at the notched section, estimated as per Equations 5.2 or 5.3, as appropriate.

[f] Total lateral load capacity of the wood section and the sprayed layer at the notched section.

For series II poles (Table 5.1), two estimated values were calculated; the combined load capacity of the wooden pole and the sprayed FRP layer at the ground line, and the load capacity of the pole only above the sprayed region. For both estimated capacities, the load capacity of the old pole was assumed as one-half that of the new pole (i.e., 0.5 P_o). The lesser of the estimated load capacities for the pole was deemed as the predicted load capacity, P_{est}, and was compared against the experimental failure load, P_{exp}.

Similarly, two values were estimated for the load carrying capacity of series III poles (Table 5.2); the lateral load capacity at the ground line, P_o, and the combined load capacity of the notched pole and the sprayed FRP layer at the notched section, where the lesser was recognized as the estimated load capacity, P_{est}, and was compared against the experimental failure load, P_{exp}. Due to the limited data available in this study on the use of NSM-GFRP bars, the contribution of those bars was not included in the load predictions.

5.2 Comparisons against Experimental Data and Model Refinement

The load predictions indicated failure above the sprayed region for all retrofitted old poles, which agreed well with the experimental observation except for O-3LP-4-L, which failed at the ground line section. This can be attributed to the fact that the estimated load capacities for that pole were close to each other. Generally, the load capacity was conservatively predicted for all old poles, where the estimated-to-experimental load ratios ranged between 0.53 to 0.68. Therefore, it was proposed to assume the load capacity of the old pole as two-thirds that of the new pole (i.e., 0.67 P_o). Based on that, the load capacities at the ground line and above the sprayed region were recalculated as $P_{pro,1}$ and $P_{pro,2}$, respectively, with the lesser taken as the estimated load capacity. This resulted in higher estimated-to-experimental load ratios, which

ranged between 0.64 to 0.91. The low ratio of 0.64 was reported for O-3LP-4-L, which failed at a much larger lateral load than any other pole, owing to the composite action of the wood and sprayed FRP, reaching the final failure at the ground line section. This may also indicate that the estimated lateral load capacity due to the sprayed FRP is conservatively estimated.

For series III poles, the load predictions indicated failure at the notched section, which was only true for the un-sprayed poles. On the other hand, all sprayed notched poles exhibited failure at the ground line section at a lateral load that lies in between the two estimated load capacities for each pole. This resulted in an estimated-to-experimental load ratio ranging between 0.71 to 0.94. The lowest ratio was observed for N-3RP-6-C, which indicates conservative prediction for the lateral load contribution of the notched pole section, sprayed FRP, or both. The simple analytical approach demonstrated above can be used for retrofitting old, decommissioned poles or repair damaged, in-service ones.

5.3 Simplified Design Model

A simplified yet conservative version of Equation 5.5 can be rearranged as shown in Equations 5.6 and 5.7 to calculate the required thickness of sprayed FRP to retrofit an old pole or a damaged new one, respectively:

$$t_{FRP} = \frac{(P_f - P_o)(L - \Delta_L)}{\pi . R^2 \cdot \phi_{FRP} f_{u,FRP}} \qquad \text{Equation 5.6}$$

$$t_{FRP} = \frac{(P_f - P_N)(L_N - \Delta_L)}{\pi . {R_N}^2 \cdot \phi_{FRP} f_{u,FRP}} \qquad \text{Equation 5.7}$$

where P_f is the factored lateral load to applied on the retrofitted pole. Further studies should investigate the optimum length for the sprayed region to achieve a reasonable lateral load capacity.

CHAPTER 6 – CONCLUSIONS AND RECOMMENDATIONS

6.1 Conclusions

In this study, the experimental results of two phases of tests, including tests on coupon, pull-off and confinement tests in addition to twelve wooden utility poles rehabilitated with sprayed-GFRP composites and NSM GFRP bars subjected to horizontal load were presented and discussed. The following conclusions were summarized from this study:

1. The tensile strength of the sprayed-GFRP composites increases non-linearly as the thickness of the sprayed GFRP layer increases.
2. With the same GFRP thickness, the compressive strength of the sprayed-GFRP composites is only slightly lower than its tensile strength.
3. The shear coupon test results indicated undesirable failure modes for the 2.5-mm thick coupons, which could have been attributed to the limited thickness which did not provide enough fibre dispersion. Consequently, no further tests were carried out with such small thickness as 2.5 mm.
4. The direct bond between wood and sprayed-GFRP composites (unsaturated polyester resin) was satisfactory. Therefore, the use of adhesives before spraying the poles was deemed unnecessary.
5. Using sprayed-GFRP composites to rehabilitate wooden utility poles is a feasible and cost-effective technique, considering the promising test results and simple application procedure demonstrated in this study. The random dispersion of the glass fibres during spraying

suggests that the resulting tensile strength can be guaranteed in the longitudinal and transverse directions.

6. With a 6-mm thick and 1.0-m (3.3-ft) long sprayed-GFRP layer centered at the ground line, the retrofitted old pole developed a load-carrying capacity that is 24% higher than the capacity required by CSA O15-15 (CSA 2019). This percentage was further increased to 28% when the layer was sprayed over a length of 2.0-m (6.6 ft), with only 500 mm below the ground line.

7. With a 4-mm thick and 2.0-m (6.6-ft) long sprayed GFRP layer, the load-carrying capacity of the retrofitted old pole was 73% higher than the load capacity required by CSA O15-15 (CSA 2019). This occurred, however, because of failure of the whole composite section (i.e., wooden pole + sprayed FRP), which may not be a desirable failure mode in practice.

8. Unlike the 4-mm thick sprayed FRP layer, using a thickness of 6 or 8 mm for the retrofitting layer shifted the failure of the old poles away from the sprayed region. However, this occurred at a relatively lower horizontal load than that of the retrofitted pole with 4-mm thick layer. This may indicate a stress concentration near the sudden transition from the retrofitted zone to the non-retrofitted one.

9. Considering that the load-carrying capacity of the retrofitted old pole did not increase as the sprayed GFRP thickness exceeded 6 mm, it is concluded that 6 mm is an adequate thickness for the sprayed GFRP to retrofit old utility poles, with the failure occurring outside the sprayed region. Further research is required to identify the optimum length of

the sprayed GFRP layer (i.e., where the strengthening effect of the sprayed GFRP layer can be better utilized).

10. With a 50% reduction in the cross-sectional area on the tension side of the pole, the sprayed-GFRP layer restored the load-carrying capacity of the damaged pole to 72% of its "at installation" one. This percentage increased further to 91% when such area reduction was on the compression side of the pole.

11. Using NSM-GFRP bars (No. 10) as the sole rehabilitation technique for the damaged wood poles was not able to restore their original capacity. Therefore, this technique is neither efficient, convenient, nor cost-effective for this application considering the time and resources needed for the installation process.

12. The combination of NSM-GFRP bars and GFRP spraying seems to be an efficient rehabilitation technique for damaged poles as it allowed the tensile-zone-notched pole to restore 94% of its at-installation capacity with a stable load-deflection response. However, a tradeoff may exist between the anticipated gain in load-carrying capacity (i.e., compared to using sprayed GFRP only) and the added complexity of installing the NSM bars.

13. A simple analytical procedure was utilized in this study for preliminary estimation of the lateral load capacity of the retrofitted poles, which resulted in reasonable and conservative estimations. This procedure was further refined for better load predictions (for the retrofitted old poles) and simple estimation of the required thickness of the sprayed GFRP layer. Further research data is required to expand the validity of the developed model, especially for damaged utility poles.

6.2 Recommendations for Future Work

Since no further research data is available on pole rehabilitation using sprayed-GFRP composites yet, considering the limitations of this study, future research is recommended in the following areas:

1. The number of tested poles is rather limited to generalize the conclusions made from this study on all wooden utility poles. Larger specimen population and a wider variety of classes and species is required.
2. A limited variety of coating thicknesses along with coating lengths were incorporated. More specimens with varied coating lengths for each thickness is required to determine the optimum length for the sprayed region and to quantify the load capacity of the sprayed GFRP (i.e., if the retrofitted poles fail by composite rupture).
3. The notched poles were retrofitted with sprayed GFRP over a limited length around the notch. A wider spectrum of coating length should be used to optimize the repairing procedure for the notched poles.
4. Only a 50% cross-sectional reduction was considered for the notched poles in this study. More percentages of cross-sectional reduction should be tested to assess the efficiency of the adopted technique in rehabilitating damaged poles.
5. Large-sized, longer, and/or more NSM-GFRP bars should be evaluated to further assess the feasibility of using NSM-GFRP bars to rehabilitate wooden utility poles.
6. The analytical model proposed was based on the limited experimental data provided herein. The accuracy of this model should be evaluated as more experimental results are reported.

REFERENCES

ACI (American Concrete Institute). 2017. *Guide for the design and construction of externally bonded FRP systems for strengthening concrete structures*. ACI PRC-440.2-17, Detroit, MI, USA.

ASTM. 2016. "Standard Test Method for Compressive Properties of Polymer Matrix Composite Materials with Unsupported Gage Section by Shear Loading (D3410)." *ASTM D3410-16*, American Society for Testing and Material, West Conshohocken, Pennsylvania, USA.

ASTM. 2017b. "Standard Test Method for Tensile Properties of Polymer Matrix Composite Materials (D3039)". ASTM D3039-17, American Society for Testing and Material, West Conshohocken, Pennsylvania, USA.

ASTM. 2017a. "Standard test methods for static tests of wood poles (D1036)". ASTM D1036-99 (R2017), American Society for Testing and Material, West Conshohocken, Pennsylvania, USA.

ASTM. 2019. "Standard Test Method for Shear Properties of Composite Materials by the V-Notched Beam Method (D5379)." ASTM D5379-19, West Conshohocken, Pennsylvania, USA.

ANSI. 1992. "Specifications and dimensions for wood poles". *ANSI 05.1*, American National Standard Institute, New York.

Bakalarz, M. M., Kossakowski, P. G., and Tworzewski, P. 2020. "Strengthening of bent LVL beams with near-surface mounted (NSM) FRP reinforcement". *Materials*, 13(10): 2350.

Banthia, N., Nandakumar, N. and Boyd, A. 2002. "Sprayed fiber-reinforced polymers:

from laboratory to a real bridge." *Concrete International*, 24(11): 47-52.

Bolin, C. A. and Smith, S. T. 2011. Life cycle assessment of pentachlorophenol-treated wooden utility poles with comparisons to steel and concrete utility poles. *Renewable & Sustainable Energy Reviews*, 15(5): 2475–2486.

Boyd, A. J. 2000. "Rehabilitation of reinforced concrete beams with sprayed glass fiber reinforced polymers". *Ph.D. Thesis*, University of British Columbia, Vancouver, Canada.

Boyd, A. J., Liang, N., Green, P. S. and Lammert, K. 2008. "Sprayed FRP repair of simulated impact in prestressed concrete girders." *Construction & building materials.* 22 (3): 411–416.

CSA (Canadian Standards Association). (2019). "Wood utility poles and reinforcing stubs", CSA O15-15 (R2019), Toronto, Ontario.

Christiansen, A. W., and Vick, C. B. 2000. "Hydroxymethylated resorcinol coupling agent for wood surfaces to produce exterior durable bonds," Silanes and Other Coupling Agents, (2): 193–208.

Crosslink Technology Inc. 2002, "Pecker Patch Attributes." *Crosslink Technology Inc. Web Page*, https://www.crosslinktech.com/downloads/pecker_patch/peckerpatch_attributes.pdf

Datla, S.V., Pandey, M. D. 2006. "Estimation of life expectancy of wood poles in electrical distribution networks. Structural Safety". 28(3): 304–319.

Deitz, D. H., Harik, I. E., and Gesund, H. 2003. "Physical properties of glass fiber reinforced polymer rebars in compression". *J. Compos. Constr.*, ASCE, 7(4): 363–366.

Dow. 1999. "DERAKANE epoxy vinyl ester resins/chemical resistance and engineering

guide." Dow Chemical Company, Midland, MI.

Eisenheld, L. 2003. "Measuring the Adhesive Bond Quality of Vinyl Ester-Glass Composites on Novolak HMR Treated Wood." *M.Sc. Thesis*, The University of Maine, Orono, Maine, USA.

El-Salakawy, E.F. and Islam, M.R. 2014. "Repair of GFRP-Reinforced Concrete Bridge Barriers". *Journal of Bridge Engineering*, ASCE, 19(6): 04014016.

Eslyn, W. E. 1970. "Utility pole decay." Wood Science and Technology, 4(2), pp.97-103

Euclid Chemical 2022. "Technical data sheet: DURAL FAST SET GEL." *The Euclid Chemical Company Web Page,* https://www.euclidchemical.com/fileshare/ProductFiles/TDS/Dural_Fast_Set_Gel.pdf

Gardner, M. 2012. "Structural Rehabilitation: Cost-effective Alternatives to Pole Replacement." *Utility Products Web Page*, https://www.utilityproducts.com/test-measurement/article/16002832/structural-rehabilitation-costeffective-alternatives-to-pole-replacement

Gentile, C. 2000. "Flexural strengthening of timber bridges using FRP." *M.Sc. Thesis*, University of Manitoba, Winnipeg, Manitoba.

Gezer, E.D. Temiz, A. and Yüksek, T. 2015. "Inspection of Wooden Poles in Electrical Power Distribution Networks in Artvin, Turkey".

Hays, W. 1986. "Extending wood pole life: solving $5-billion/year program." *Electrical World*, pp. 41-47.

Hussain, Q. and Pimanmas, A. 2015. "Shear strengthening of RC deep beams with openings using Sprayed Glass Fiber Reinforced Polymer Composites (SGFRP) : Part 1.

Experimental study". KSCE Journal of Civil Engineering, 19(7), 2121–2133.

Johns, K. C. and Lacroix, S. 2000. "Composite reinforcement of timber in bending." *Canadian Journal of Civil Engineering*, 27 (5), 899–906.

Kell, J. A. 2001. "Repair of wooden utility poles using fibre-reinforced polymers." MSc Thesis, University of Manitoba, Winnipeg, Canada.

Laminated Wood Systems 2013. "PRH Installation Manual." *Laminated Wood Systems Web Page*, https://www.lwsinc.com/sites/default/files/files/PRH%20Installation%20Manual.pdf.

Laminated Wood Systems 2014. "PRS Brochure 11-15." *Laminated Wood Systems Web Page*, https://www.lwsinc.com/sites/default/files/files/PRS%20Brochure%2011-15.pdf.

Laminated Wood Systems 2017. "Pole Repair Canada." *Laminated Wood Systems Web Page*, https://www.lwsinc.com/sites/default/files/files/Pole%20Repair%20Canada.pdf.

Lee, K. S., Lee, B. Y., and Seo, S. Y. 2016. "A Seismic Strengthening Technique for Reinforced Concrete Columns Using Sprayed FRP." *Polymers*. 8 (4): 107.

Lopez-Anido, R., Michael, A. P. and Sandford, T. C. 2003. "Experimental characterization of FRP composite-wood pile structural response by bending tests". *Marine structures*. 16 (4), 257–274.

LRBG Chemicals Inc. 2023. "PRF Resins." *LRBG Chemicals Inc. Web Page*, https://lrbgchemicals.com/prf-resins/.

Manitoba Hydro 2012. "REPORT ON Distribution Asset Condition", *Manitoba Hydro Web Page*, https://www.hydro.mb.ca/docs/regulatory_affairs/pdf/gra_2012_2013/Appendix_40.pdf

McGuire, J. M., Lynch, O. J., Schneider, V., Bingel, N. G., Reay, J. and Wachholz, T. 2019. Wood Pole Structures for Electrical Transmission Lines: Recommended Practice for Design and Use. Book published by American Society of Civil Engineers.

Merschman, E., Salman, A. M., Bastidas-Arteaga, E., and Li, Y. 2020. "Assessment of the effectiveness of wood pole repair using FRP considering the impact of climate change on decay and hurricane risk." *Advances in climate change research.*

Mohit, S.A. and El-Salakawy, E.F. 2019. "Rehabilitation of Reinforced Concrete Circular Columns with Sprayed Glass Fiber Reinforced Polymer (GFRP) Composites." ASCE, Journal of Composites for Construction, 23(6): 04019045.

Morrell, J. J. 2016. "Estimated Service Life of Wood Poles." *North American Wood Pole Council Web Page*, https://woodpoles.org/portals/2/documents/TB_ServiceLife.pdf.

North American Wood Pole Council (NAWPC). 2021. "How Poles Are Made," *North American Wood Pole Council Web Page*, https://woodpoles.org/Why-Wood-Poles/How-Poles-Are-Made.

Osmose 2020. "FiberWrap II brochure 2020." *Osmose Web Page*, https://f.hubspotusercontent30.net/hubfs/20067784/Osmose_Nov2021/pdf/FiberWrap%20sell%20sheet%20-%202020%20-%20FINAL.pdf

Osmose 2022. "Pole Restoration brochure 2022." *Osmose Web Page*, https://info.osmose.com/hubfs/Pole%20Restoration%20sell%20sheet%20-%202022%20FINAL%20(1).pdf

Parghi, A. and Alam, M. S. 2018. "A review on the application of sprayed-FRP composites for strengthening of concrete and masonry structures in the construction sector".

Composite structures. 187, 518–534.

Plevris, N., and Triantafillou, T. C. 1992. "FRP-Reinforced Wood as Structural Material". *Journal of materials in civil engineering*. 4 (3), 300–317.

Polywater 2019. "Polywater Pole Repair Sealant (UPR-PR) Instructions." *Polywater Web Page*, https://www.polywater.com.

Polyzois, D. and Kell, J. A. 2007. "Repair and rehabilitation of wood utility poles with fibre-reinforced polymers." *Canadian Journal of Civil Engineering*. 34 (1), 116–119.

Pultrall Inc. 2019. "V-ROD—Technical data sheet." ADS Comp. Group. Thetford Mines, QC, Canada.

Rotafix Northern Ltd. 2023. "Rotafix Structural Adhesive (RSA) Data Sheet." http://rotafix.co.uk/products/timber-engineering/rotafix-structural-adhesive/.

Saafi, M. and Asa, E. 2010. "Extending the Service Life of Electric Distribution and Transmission Wooden Poles Using a Wet Layup FRP Composite Strengthening System". ASCE, *Journal of Performance of Constructed Facilities.* 24 (4): 409–416.

Superior Polymer. 2000. "Technical data sheet: Hydrobond 500 underwater epoxy adhesive." Superior Polymer Products, Calumet, MI.

Talukdar, S. and Banthia, N. 2010. "Performance of Sprayed Fiber Reinforced Polymer Strengthened Timber Beams". *Advances in materials science and engineering*: 1–6.

Tavassoli, A., Liu, J., and S. Sheikh. 2015. "Glass fiber-reinforced polymer-reinforced circular columns under simulated seismic loads"**.** *ACI Struct. J.* 110 (6): 941–951.

Thermo Fisher Scientific UK 2020. "CAB-O-SIL M5 Safety Data Sheet." https://assets.thermofisher.com/DirectWebViewer/private/document.aspx?prd=ACR40373~~

PDF~~MTR~~CLP1~~EN~~2020-12-21%2019:51:20~~CAB-O-SIL%c2%ae%20M5~~.

TPI. 2001. “An overview of the SCRIMP™ technology.” TPI Technology, Inc., Warren, RI.

Wang, C-H., Leicester, R. H. and Nguyen, M. N. 2008. “Manual No. 3: decay in ground contact.” *Forest & Wood Products Australia*.

Yang, Z., Wu, Kun., and Edalati, K. 2016. “Experimental Analysis of Tensile Mechanical Properties of Sprayed FRP”. *Advances in Materials Science and Engineering.* Vol. 2016, pp.1–12.

Yeboah, D., and Gkantou, M. 2021. “Investigation of flexural behaviour of structural timber beams strengthened with NSM basalt and glass FRP bars.” *Structures*, 33: 390-405.